Long-term climate change commitment and reversibility: an EMIC intercomparison

Journal Item

Version: Accepted Manuscript

Link(s) to article on publisher's website:
http://dx.doi.org/doi:10.1175/JCLI-D-12-00584.1

AMERICAN METEOROLOGICAL SOCIETY

Journal of Climate

EARLY ONLINE RELEASE

The DOI for this manuscript is doi: 10.1175/JCLI-D-12-00584.1

Long-term Climate Change Commitment and Reversibility: An EMIC Intercomparison

Kirsten Zickfeld *

Department of Geography, Simon Fraser University, Burnaby, BC, Canada

Michael Eby, Kaitlin Alexander, Andrew J. Weaver

School of Earth and Ocean Sciences, University of Victoria, Victoria, BC, Canada

Elisabeth Crespin, Thierry Fichefet, Hugues Goosse

Gwenaëlle Philippon-Berthier

Université Catholique de Louvain, Earth and Life Institute,

Georges Lemaître Centre for Earth and Climate Research, Louvain-La-Neuve, Belgium

Neil R. Edwards, Philip B. Holden

The Open University, Milton Keynes, United Kingdom

Alexey V. Eliseev, Igor I. Mokhov

A.M. Obukhov Institute of Atmospheric Physics, RAS, Moscow, Russia

Georg Feulner, Hendrik Kienert, Mahé Perrette

Thomas Schneider von Deimling

Potsdam Institute for Climate Impact Research, Potsdam, Germany

9 Chris E. Forest

Pennsylvania State University, College Park, Pennsylvania, USA

10 Pierre Friedlingstein

University of Exeter, Exeter, UK

11 Fortunat Joos, Renato Spahni, Marco Steinacher

Physics Institute, University of Bern, Bern, Switzerland

Oeschger Centre for Climate Change Research, University of Bern, Bern, Switzerland

12 Michio Kawamiya, Kaoru Tachiiri

Research Institute for Global Change, JAMSTEC, Yokohama, Japan

13 David Kicklighter

The Ecosystems Center, MBL, Woods Hole, Massachusetts, USA

14 Erwan Monier, Adam Schlosser, Andrei Sokolov

Massachusetts Institute of Technology, Cambridge, Massachusetts, USA

15 Katsumi Matsumoto, Kathy S. Tokos

University of Minnesota, Minneapolis, Minnesota, USA

16 Steffen M. Olsen

Danish Meteorological Institute, Copenhagen, Denmark

17 Jens O. P. Pedersen

National Space Institute, Technical University of Denmark, Kgs. Lyngby, Denmark

18 Andy Ridgwell

School of Geographical Sciences, University of Bristol, Bristol, United Kingdom

19 Gary Shaffer

Department of Geophysics, University of Concepcion, Concepcion, Chile

Niels Bohr Institute, University of Copenhagen, Copenhagen, Denmark

20 Masakazu Yoshimori

University of Tokyo, Tokyo, Japan

21 Ning Zeng, Fang Zhao

University of Maryland, College Park, Maryland, USA

Corresponding author address: Kirsten Zickfeld, Department of Geography, Simon Fraser University, 8888 University Drive, Burnaby, BC, V5A1S6.

E-mail: kzickfel@sfu.ca

ABSTRACT

This paper summarizes the results of an intercomparison project with Earth System Models of Intermediate Complexity (EMICs) undertaken in support of the Intergovernmental Panel on Climate Change (IPCC) Fifth Assessment Report (AR5). The focus is on long-term climate projections designed to: (i) quantify the climate change commitment of different radiative forcing trajectories, and (ii) explore the extent to which climate change is reversible on human timescales. All commitment simulations follow the four Representative Concentration Pathways (RCPs) and their extensions to 2300. Most EMICs simulate substantial surface air temperature and thermosteric sea level rise commitment following stabilization of the atmospheric composition at year-2300 levels. The meridional overturning circulation (MOC) is weakened temporarily and recovers to near pre-industrial values in most models for RCPs 2.6–6.0. The MOC weakening is more persistent for RCP 8.5. Elimination of anthropogenic CO_2 emissions after 2300 results in slowly decreasing atmospheric CO_2 concentrations. At year 3000 atmospheric CO_2 is still at more than half its year-2300 level in all EMICs for RCPs 4.5–8.5. Surface air temperature remains constant or decreases slightly and thermosteric sea level rise continues for centuries after elimination of CO_2 emissions in all EMICs. Restoration of atmospheric CO_2 from RCP to pre-industrial levels over 100–1000 years requires large artificial removal of CO_2 from the atmosphere and does not result in the simultaneous return to pre-industrial climate conditions, as surface air temperature and sea level response exhibit a substantial time lag relative to atmospheric CO_2.

1. Introduction

This paper summarizes the results of a model intercomparison project undertaken in support of the Fifth Assessment Report (AR5) of the Intergovernmental Panel on Climate Change (IPCC). Fifteen groups running Earth System Models of Intermediate Complexity (EMICs) participated in the intercomparison. Coordinated experiments include simulations of the climate of the past millennium and simulations of long-term future climate change, in addition to a set of idealized experiments. This paper will discuss the future climate projections, while the idealized and last-millennium simulations are the focus of a separate paper (Eby et al. 2013). The goals of the future climate simulations are to: (i) quantify the long-term climate change commitment in response to different radiative forcing trajectories, and (ii) explore the extent to which climate change is reversible if atmospheric CO_2 is left to evolve freely or is artificially restored to pre-industrial levels.

Climate change commitment refers to the climate changes that are to be expected in the future in response to past human activities. The concept of commitment is tied to the thermal inertia of the climate system (Hansen et al. 1985), which causes the effects of greenhouse gas emissions to be felt beyond the duration of those emissions. Climate change commitment is a useful metric for climate science and policy, as it quantifies the minimum climate change humanity faces, and represents a benchmark against which to measure the effect of future emissions. Most studies consider the "warming commitment", but here we use the broader term "climate change commitment" to include other aspects of climate change such as sea level rise (Wigley 2005).

Different forms of climate change commitment have been discussed in the literature. The most prominent is the "constant composition" commitment, which refers to the climate changes that are to be expected after stabilization of the chemical composition of the atmosphere, and hence the radiative forcing, at a specified level (Wigley 2005; Meehl et al. 2005; Hare and Meinshausen 2006). This commitment was highlighted in the IPCC Fourth Assessment Report (AR4) and has been estimated at between 0.3°C and 0.9°C for the period

2090–2099 relative to 1980–1999 if the atmospheric composition is stabilized at year 2000 levels (Meehl et al. 2007).

Another type of commitment, which has received greater attention more recently, is the "zero-emissions" commitment, which is the warming that is to be expected after complete elimination of emissions (Hare and Meinshausen 2006; Matthews and Caldeira 2008; Plattner et al. 2008; Eby et al. 2009; Lowe et al. 2009; Froelicher and Joos 2010; Solomon et al. 2010; Gillett et al. 2011; Zickfeld et al. 2012; Matthews and Zickfeld 2012). Most studies have explored the climate response to elimination of CO_2 emissions only. These studies have shown that instantaneous elimination of CO_2 emissions results in approximately constant global mean temperature for several centuries after emissions cease. When emissions of non-CO_2 greenhouse gases and aerosols also cease (Hare and Meinshausen 2006; Solomon et al. 2010; Froelicher and Joos 2010; Armour and Roe 2011; Matthews and Zickfeld 2012), the climate warms for about a decade and then gradually cools. The initial warming is due to the fast elimination of the negative radiative forcing associated with aerosols, which have a short atmospheric residence time. Greenhouse gases, on the other hand, have a longer atmospheric lifetime and their concentration and associated radiative forcing decline gradually after elimination of emissions. After about a century, the response is largely dominated by the long-lived CO_2 and the rate of cooling converges to that obtained under elimination of CO_2 emissions alone. Matthews and Weaver (2010) argue that the zero emission commitment is a more useful measure of climate change commitment, because it does not convolute the physical response of the climate system to past emissions with the response to future emissions that are needed to maintain the atmospheric CO_2 concentration at stable levels, as for the constant composition commitment.

Another form of climate change commitment is the "constant emissions" commitment, which refers to the climate changes to be expected in response to constant anthropogenic emissions (Wigley 2005; Hare and Meinshausen 2006; Meinshausen et al. 2011b). This type of commitment is less prominently discussed in the literature. A study with a simple climate

model (MAGICC) calibrated to Atmosphere-Ocean General Circulation Models (AOGCMs) (Meinshausen et al. 2011a) estimates the constant emissions commitment at 1–2.5°C by 2100 (relative to 2000) assuming constant year-2010 emissions (Collins et al. 2013).

The second set of experiments which is part of this model intercomparison is aimed at exploring the extent to which the climate system can revert to "safe" levels, should climate change impacts turn out to be "dangerous". Insight gained from zero emission commitment simulations suggests that because of the long residence time of CO_2 in the atmosphere (Archer and Brovkin 2008; Eby et al. 2009) and the large thermal reservoir of the ocean, complete elimination of emissions can at best lead to stable or slowly decreasing temperatures. If permafrost carbon feedbacks are considered, elimination of emissions could lead to a continuing increase in temperature (MacDougall et al. 2012). Therefore, restoring temperature to lower levels in a time frame meaningful to human societies can only be accomplished with "negative emissions" i.e. net removal of carbon dioxide from the atmosphere. Such negative emissions can be achieved, for instance, by biomass energy in combination with capture and geological storage of the emitted CO_2 (BECS) (Azar et al. 2006), or by CO_2 "scrubbers" which remove the CO_2 directly from the atmosphere (Keith et al. 2006).

Few studies to date have explored the response of the climate system to scenarios with negative emissions or "overshoot" scenarios (Yoshida et al. 2005; Tsutsui et al. 2007; Nusbaumer and Matsumoto 2008; Zickfeld et al. 2012). Most of these studies use idealized scenarios, such as atmospheric CO_2 increasing gradually to two or four times the pre-industrial level and then decreasing at a similar rate (Held et al. 2010; Boucher et al. 2012). These studies suggest that because of the long timescales of components of the climate system, global mean temperature, precipitation, ocean heat content and other quantities lag the forcing and revert to the target level only slowly. The residual change (i.e. the difference between the target and the actual level) increases with the level of peak forcing (Held et al. 2010; Boucher et al. 2012). The idealized scenarios used in these papers, which entail large and abrupt decreases in atmospheric CO_2, imply levels of negative emissions that are likely beyond known

technological capabilities (McGlashan et al. 2012). The set of scenarios used for the Coupled Model Intercomparison Project Phase 5 (CMIP5) (Taylor et al. 2008) includes one scenario with moderate negative emissions which is based on plausible technological and economic assumptions (Representative Concentration Pathway (RCP) 2.6; Moss et al. (2010)).

In this paper, we analyze multi-century constant composition, zero emissions and constant emissions commitment simulations with EMICs under a range of radiative forcing scenarios. In addition, we investigate the EMICs' response to a set of reversibility scenarios, whereby atmospheric CO_2 is artificially restored to pre-industrial levels, or is left to evolve freely after a millennium of constant radiative forcing. Finally, we explore the cumulative CO_2 emissions that are compatible with climate stabilization targets using inverse simulations with two EMICs.

The paper is organized as follows. In Section 2 we briefly introduce the EMICs that participated in the model intercomparison and describe the experimental setup. In Section 3 the results of the model simulations are presented and discussed with reference to the literature. The section starts with a discussion of the ability of EMICs to simulate the climate of the 20^{th} century, continues with a description of the results of the climate change commitment and reversibility simulations and ends with a discussion of cumulative emissions compatible with long-term climate targets. Section 4 presents a summary and conclusions.

2. Methods

a. Participating Models

This study includes results from twelve EMICs, eight of which are coupled climate-carbon cycle models. The models are the University of Bern three-dimensional Earth system model (Bern3D-LPJ) (Ritz et al. 2011; Stocker et al. 2011), versions 2.4 and 3α of the Potsdam Institute climate and biosphere model (CLIMBER-2.4, CLIMBER-3α) (Petoukhov et al. 2000; Montoya et al. 2005), version 1.0 of the Danish Centre for Earth System Science

(DCESS) Earth System model (Shaffer et al. 2008), release 2-2-7 of the GENIE Earth system model adapted with an implementation of land use change (Holden et al. 2013), the A.M Obukhov Institute of Atmospheric Physics, Russian Academy of Sciences climate model (IAP RAS CM) (Eliseev and Mokhov 2011), version 2.2 of the Massachusetts Institute of Technology's Integrated Global System Model (IGSM2.2) (Sokolov et al. 2005), version 1.2 of the LOVECLIM Earth System Model (LOVECLIM 1.2) (Goosse et al. 2010), version 1.0 of the MESMO Earth System Model (MESMO 1.0) (Matsumoto et al. 2008), the MIROC-lite-LCM Earth System model (Tachiiri et al. 2010), version 2.0 of the University of Maryland Coupled Atmosphere-Biosphere-Ocean model (UMD 2.0) (Zeng et al. 2004), and version 2.9 of the University of Victoria Earth System Climate Model (UVic 2.9) (Weaver et al. 2001; Eby et al. 2009). The characteristics of each model are briefly described in the EMIC intercomparison companion paper (Eby et al. 2013).

A common trait of these models is that they are simplified, i.e. include processes in a more parameterized form and have generally lower resolution compared to atmosphere-ocean general circulation models (AOGCMs) and complex Earth System Models (ESMs). The group of EMICs, however, is very heterogeneous, ranging from zonally averaged (Petoukhov et al. 2000) or mixed layer ocean models (Sokolov et al. 2005) coupled to statistical-dynamical models of the atmosphere to low-resolution three-dimensional ocean general circulation models coupled to simplified dynamical models of the atmosphere (Goosse et al. 2010). Eight out of twelve models include an interactive carbon cycle (Bern3D-LPJ, DCESS, GENIE, IGSM2.2, MESMO, MIROC-lite-LCM, UMD, UVic 2.9). Of these, several models calculate land-use emissions internally (Bern3D-LPJ, GENIE, IGSM,UVic 2.9) and/or represent seafloor sediment processes, including deep water carbonate sedimentation (Bern3D-LPJ, DCESS, GENIE, UVic 2.9).

b. Experimental Design

Most models were spun up with year-850 forcing. The models were then integrated from 850 to 2005 using known natural (orbital, volcanic, solar) and anthropogenic (greenhouse gas, aerosol, land-cover change) forcing, following the PMIP3/CMIP5 protocol. Details on the implementation of these forcings in individual EMICs is provided in the Appendix of the EMIC intercomparison companion paper (Eby et al. 2013). Note that in this paper we only consider the 1850–2005 portion of the last millennium simulation (henceforth referred to as the "historical" or HIST simulation). The full simulation is discussed in detail in Eby et al. (2013). The MIROC-lite-LCM model was spun up with year-1850 forcing and integrated from 1850 to 2005.

Starting from the end point of the historical simulation, models were integrated with CO_2 concentration and non-CO_2 greenhouse gas forcing specified according to four Representative Concentration Pathways (RCPs) (from 2006 to 2100) and their extensions (to 2300) (Meinshausen et al. 2011b). Aerosol forcing (direct effect) and land-cover change followed RCP specifications until 2100 and were held constant thereafter. Natural forcings were specified as follows: orbital forcing was held fixed at year-2005 levels, solar irradiance was set to repeat the last solar cycle (1996–2008) and volcanic forcing was set to zero.

The atmospheric CO_2 concentration of the four RCPs (RCP2.6, RCP4.5, RCP6.0, RCP8.5) and their extensions is shown in Figure 1.

From year 2301 to 3000 a set of climate change commitment simulations was performed for all four RCPs. In the constant composition commitment (CCO) simulations, atmospheric CO_2 concentration and the forcing from non-CO_2 greenhouse gases were held constant at year-2300 levels. Other forcings were held fixed at the level specified for the RCP simulations. A slightly different simulation protocol was followed for the MIROC-lite-LCM, with constant solar forcing after 2300 (no solar cycle). EMICs with a carbon cycle diagnosed the CO_2 emissions compatible with the specified CO_2 concentration trajectories.

The commitment runs described in the following were performed with climate-carbon

cycle models only. In a second set of simulations, which we designate as the "pre-industrial CO_2 emission commitment" experiments (PIEM-CO_2), the "anthropogenic CO_2 perturbation" - defined as the difference in implied CO_2 emissions between the last decade of the RCP simulations (2290–2300) and the decade 1840–1850 of the historical simulation - was set to zero starting in 2300, while the radiative forcing from non-CO_2 greenhouse gases was held fixed at year-2300 levels. Other forcings were held fixed at the level specified for the RCP simulations. For the GENIE model, CO_2 emissions were set to zero after 2300. It should be noted that in most models, setting the anthropogenic perturbation to zero did not result in zero emissions exactly. The reason is that the 1840–1850 land-atmosphere and ocean-atmosphere CO_2 fluxes in response to forcing are not exactly consistent with the specified atmospheric CO_2. Diagnosed emissions are negative in all models (except UMD), implying a flux of CO_2 from the land and ocean into the atmosphere. Processes responsible for the excess emissions could be the warming recovery after volcanic eruption, or land use change.

In the pre-industrial emission simulations (PIEM), CO_2 emissions after 2300 were specified as in the PIEM-CO_2 simulation, but the radiative forcing from non-CO_2 greenhouse gases was set to 1840–1850 average levels. Other forcings were held fixed at the level specified for the RCP simulations.

In the constant emissions commitment (CEM) simulations, implied CO_2 emissions over the last decade of the RCP integrations (years 2290-2300) were diagnosed, and CO_2 emissions held fixed at this value from 2300 onwards. Radiative forcing from non-CO_2 greenhouse gases was held constant at year-2300 levels and other forcings were held fixed at the level specified for the RCP simulations.

In addition to the commitment simulations, a set of reversibility runs (RE) was also performed by several EMIC groups. These simulations start from the year-3000 model configuration of the constant composition commitment (CCO) experiments and extend to the year 4000. In the first experiment (REa), atmospheric CO_2 decreases linearly to the pre-industrial level over 100 years, while non-CO_2 forcings are held fixed at year-3000 lev-

els. Forcing specifications are similar in the second experiment (REb), except that CO_2 is prescribed to decrease to pre-industrial levels over a period of 1000 years. In the third experiment (REc), atmospheric CO_2 is allowed to evolve freely (zero CO_2 emissions) and non-CO_2 forcings are again held fixed at year-3000 levels. REc experiments with freely evolving atmospheric CO_2 were performed by EMICs with an interactive carbon cycle only.

Finally, a set of simulations was carried out whereby a temperature stabilization trajectory was specified, and the cumulative emissions consistent with that temperature trajectory were calculated, following the inverse modelling approach described in Zickfeld et al. (2009). Four "temperature tracking" (TTR) simulations were performed, with global mean surface air temperatures stabilizing at 1.5°C, 2°C, 3°C and 4°C warming relative to pre-industrial. The simulations started from the end of the historical simulation and were integrated to year 2500. Natural forcings were specified as in the RCP simulations. Land-use change was held constant at the year-2005 pattern, whereas non-CO_2 greenhouse gas and aerosol forcing linearly decreased from year-2005 values to zero by 2300.

All model simulations are summarized in Table 1.

3. Results and Discussion

a. Historical simulation

The performanace of EMICs over the historical period is discussed in detail in Eby et al. (2013). Here, we briefly summarize the main findings to allow the reader to put the EMICs' future projections and their uncertainty ranges into perspective.

Over the 20^{th} century EMICs simulate a model ensemble mean warming of 0.78°C (range: 0.4–1.2°C), compared to the observed warming of 0.73°C (Morice et al. 2013) over the same period (Table 2). Five models stay mostly within the observational uncertainty envelope for this period, five tend to overestimate the observed warming and two tend to underestimate it (Eby et al. (2013), Figure 1b). The spread in models is due to different climate sensitivities

and differences in the specification of radiative forcing, particularly from land-use change and tropospheric aerosols (Eby et al. 2013).

EMICs simulate a model-mean rate of ocean thermal expansion for 1971–2010 of 1.1 mm yr^{-1} compared to the observations-based estimate of 0.8 mm yr^{-1} (Rhein et al. 2013). Eight EMICs are within the uncertainty range of observed values, and four overestimate thermal expansion. Ocean thermal expansion is determined by both the models' heat uptake efficacy and climate sensitivity, which differ largely between models (Eby et al. 2013, Table 2).

The atmospheric CO_2 concentration was specified in the historical simulation and EMICs with an interactive carbon cycle were used to diagnose the CO_2 emissions compatible with the specified CO_2 concentrations. The average EMIC carbon cycle response for the 1990s is within the uncertainty range of observed values (Denman et al. 2007), except for diagnosed emissions, which are slightly underestimated (Table 2). Ocean fluxes simulated by all but one EMICs are within the uncertainty range of observed values. Although the EMIC average land fluxes fall within the large range of uncertainty, several models underestimate both the land use change flux and the residual land flux (i.e. the total land-atmosphere flux minus the land use change flux).

The EMICs' cumulative carbon fluxes from 1800 to 1994 are compared to estimates from Sabine et al. (2004). Again, all models estimate total ocean uptake within the uncertainty range of observed values (Table 2). Land uptake differs largely between models, with only half of the models' simulated fluxes falling within the estimated uncertainty range. EMICs whose land flux agrees well with observation also simulate 1800–1994 cumulative emissions within the observed range.

Overall, the 20^{th} century climate and carbon cycle response simulated by EMICs agrees reasonably well with observations, which supports the use of EMICs to project long-term climate change and to complement more complex AOGCMs and Earth System models.

b. Constant composition commitment

Figure 2 shows the time evolution of physical climate variables for the constant composition commitment simulations. At the multi-century time scale considered in this study, the warming depends strongly on the forcing scenario, being highest in RCP8.5 and lowest in the low emission RCP2.6 scenario. Following the radiative forcing, the model ensemble mean temperature under the RCP2.6 scenario peaks at 2070 and declines until reaching a minimum in 2300, after which it slowly increases again. Global mean temperature under RCP2.6 peaks at 1.0°C relative to 1986–2005 in the ensemble mean (model range: 0.6–1.5°C) and decreases to 0.6°C (0.3–1.1°C) at 2300. Assuming an observed warming of 0.7°C between 1850 and 2005, the ensemble mean peak and year-2300 warming are 1.7°C and 1.3°C above pre-industrial, respectively. In a few models, however, peak warming exceeds 2.0°C relative to preindustrial (Fig. 3).

Under the other RCP scenarios (RCP4.5, RCP6.0, RCP8.5) the global temperature increases rapidly until the time of stabilization of the forcing, and more slowly thereafter. By 2300, global warming approaches 2.2°C under RCP4.5, 3.3°C under RCP6.0, and 7.0°C under RCP8.5 in the ensemble mean (relative to 1986–2005). The ensemble means and model ranges are generally consistent with those simulated by AOGCMs and Earth System models contributing to the CMIP5 (Table 3).

Most EMICs simulate a considerable warming commitment following stabilization of radiative forcing at year-2300 levels. The continuing albeit slower warming after stabilization is a well known feature of climate models and is associated with the large thermal inertia of the ocean (Hansen et al. 1985). IPCC AR4 models estimated the additional warming after stabilization of the atmospheric composition at year-2000 levels at 0.6°C for the period 2090–2099 relative to 1980–1999 (Meehl et al. 2007), or 0.3°C relative to 2000 (Collins et al. 2013). AOGCM simulations in support of IPCC AR5 do not include a year-2000 constant composition commitment simulation. It is possible, however, to estimate the warming commitment for the RCP4.5 scenario and its extension: it amounts to 0.8°C between 2100

(the time of stabilization of the radiative forcing) and 2300 (Collins et al. 2013, Table 12.2). In this study the model mean warming between 2100 and 2300 is 0.3–0.4°C for RCPs 4.5, 6.0 and 8.5, somewhat lower than the CMIP5 estimate. The additional warming between 2300 and 3000 is 0.3°C, 0.4°C and 0.7°C in the ensemble mean for RCPs 4.5, 6.0 and 8.5, respectively, indicating a slight increase with radiative forcing. Another measure of constant composition commitment is the fraction of realized warming (Solomon et al. 2009), which is here estimated as the ratio of warming at a given time to the warming averaged over the last two decades of the simulation (2981–3000) (Fig. 2). At the time of stabilization of radiative forcing, the fraction of realized warming is ∼70–90% in the ensemble mean for RCPs 4.5, 6.0 and 8.5.

Sea level rise due to thermal expansion ("thermosteric" sea level rise) continues for centuries after stabilization of radiative forcing in all scenarios due to the long response time scale of the deep ocean. Despite the peaking and declining radiative forcing under RCP2.6, the rate of thermosteric sea level rise is positive throughout the duration of the simulation in all models (Fig 2). Thermal expansion simulated by EMICs for the four RCPs and selected time periods is given in Table 3. The model mean thermal expansion by 2100 agrees very well with that simulated by CMIP5 models.

The thermosteric sea level rise commitment after stabilization of radiative forcing is substantial under RCPs 4.5, 6.0 and 8.5 and at 3000 amounts to 1.5–3 times the thermosteric sea level rise at the time of forcing stabilization. Note that none of the EMICs include sea level rise due to melting of land-based glaciers and ice sheets. Consideration of these contributions would lead to substantially higher sea level rise estimates, but the exact value is highly uncertain due to incomplete understanding of glacier and ice sheet dynamics.

The Atlantic meridional overturning circulation (MOC) weakens under all scenarios (Fig. 2). Under RCPs 2.6, 4.5 and 6.0 the weakening is temporary, and the circulation recovers to within 80% of the pre-industrial strength at the end of the simulation in most models. Under RCP8.5 the weakening is more persistent, and the model ensemble mean

MOC recovers to 60% of the pre-industrial strength at 3000. Under this scenario the MOC response varies considerably among models: while in some models the circulation recovers to near pre-industrial values, it is close to a complete collapse in the Bern3D-LPJ EMIC.

Comparison of constant composition commitment estimates with those from an earlier EMIC intercomparison (Plattner et al. 2008) is hampered by the use of different scenarios (SRES as opposed to RCP) and set of models used. However, given the similarity of the SRES B1 stabilization scenario and RCP 4.5 (in both scenarios atmospheric CO_2 stabilizes at 550 ppmv) we attempted a comparison of the warming and thermal expansion commitment for these two scenarios. The additional warming between years 2100 and 3000 is larger in Plattner et al. (2008) than in this study (0.6–1.6°C for SRES B1 versus 0.1–1.2°C for RCP 4.5), but with a similar inter-model range ($\sim$1.0°C). Thermal expansion commitment is similar in the two studies, with the range simulated in this study ecompassing the range of Plattner et al. (2008) (0.3–1.1 m for SRES B1 versus 0.2–1.4 m for RCP 4.5). Differences in warming and thermal expansion commitment may be due to the different set of models used in the two intercomparisons, but also differences in non-CO_2 forcing between scenarios.

EMICs with an interactive carbon cycle were used to diagnose the CO_2 emissions compatible with the CO_2 concentration pathways specified under the constant composition commitment simulations. Diagnosed CO_2 emissions are estimated by closing the global-mean carbon budget of the atmosphere and are determined by the atmosphere-land and atmosphere-ocean CO_2 fluxes. Figure 4 shows CO_2 emissions and changes in carbon inventories since 1850 simulated by eight EMICs for scenario RCP2.6. CO_2 emissions peak around 2020, and decline steeply thereafter. Since the rate of atmospheric CO_2 decrease exceeds the rate of CO_2 uptake by carbon sinks, diagnosed emissions become negative in all models. Minimum emissions range from -1.5 $PgCyr^{-1}$ to -0.5 $PgCyr^{-1}$. After stabilization of atmospheric CO_2, emissions settle at a slightly positive value (equal to the rate of CO_2 uptake by carbon sinks). Cumulative CO_2 emissions since 1850 vary substantially among models despite identical prescribed atmospheric CO_2 and range from 300 PgC to 830 PgC at 2300 and from

380 PgC to 1040 PgC at year 3000. The airborne fraction of cumulative emissions decreases from 45–70% at the time of peak atmospheric CO_2 (year 2050) to 15–42% at the end of the simulation.

Accumulated land carbon uptake is negative at the year 2000 in all models that simulate land use change (LUC) emissions interactively on the basis of land cover changes (all EMICs except MESMO, UMD). The reason is that CO_2 emissions due to land-use exceed net CO_2 uptake by vegetation during most of the historical period (Eby et al. 2013). Between 2000 and the year of peak atmospheric CO_2, the terrestrial biosphere acts as a sink of CO_2 in most models (except in Bern3D-LPJ and UVic). Between the CO_2 peak and the time of CO_2 stabilization, the terrestrial biosphere becomes a source of CO_2 in all models. The range in land carbon uptake under the RCP2.6 scenario is spanned by the UMD model at the upper end, which has a small land uptake sensitivity to CO_2 (β_L) but also a small sensitivity to temperature (γ_L) (Eby et al. 2013) and does not simulate LUC emissions, and the Bern3D-LPJ and UVic models at the lower end (both models have large land uptake sensitivities to CO_2 but also medium to large sensitivities to temperature and do simulate LUC emissions). The fraction of cumulative emissions taken up by the land (land uptake fraction) decreases between 2100 and 2300 and remains approximately constant thereafter.

The ocean takes up carbon from the atmosphere throughout the duration of the RCP 2.6 constant composition simulation in all models. Ocean carbon uptake slows after the peak in atmospheric CO_2 and accelerates again after CO_2 is stabilized. Accumulated ocean carbon uptake is larger than accumulated land carbon uptake at all times in all models. The range in ocean carbon uptake is spanned by the UMD model at the upper end (highest ocean carbon uptake sensitivity to CO_2, γ_O; Eby et al. (2013)) and the UVic model (low carbon uptake sensitivity to CO_2). The ocean uptake fraction increases continuously between the time of peak CO_2 and 2300, and remains approximately constant thereafter.

Figure 5 displays changes in carbon inventories in the year 3000 for constant composition commitment simulations under all four RCPs. Diagnosed cumulative CO_2 emissions increase

approximately linearly with atmospheric CO_2 for RCPs 2.6–6.0, but the increase becomes less than linear at higher radiative forcing in most models. The spread in cumulative emissions diagnosed by models also increases with higher atmospheric CO_2, with a range as large as 4,500–11,500 PgC for RCP8.5. Cumulative emissions at the upper end of this range are close to estimates of the carbon bound in the total fossil fuel resource base (9,500–15,600 PgC; GEA (2012)).

The airborne fraction increases with increasing atmospheric CO_2, from a model ensemble mean of 0.27 for RCP2.6 to 0.57 for RCP8.5. The increase in airborne fraction with CO_2 is mostly a result of the decreasing ocean uptake fraction.

Ocean carbon uptake is largely driven by atmospheric CO_2, with the lowest cumulative uptake occurring in RCP2.6 and the largest in RCP8.5. The ocean uptake fraction decreases significantly with higher CO_2 in all models, from an ensemble mean value of 0.89 in RCP2.6 to 0.44 in RCP8.5. The decrease in ocean uptake fraction is due to nonlinear ocean carbonate chemistry and stronger climate-carbon cycle feedbacks at higher atmospheric CO_2 (Friedlingstein et al. 2006; Plattner et al. 2008).

The results for land carbon uptake are more complex, as they vary significantly across models and scenarios. In RCPs 4.5 and 6.0, the terrestrial biosphere takes up carbon between 2000 and the year of CO_2 stabilization in all models (not shown). In RCP8.5, the terrestrial biosphere initially takes up CO_2, but becomes a CO_2 source after about a century in most models. The Bern3D-LPJ exhibits negligible land uptake even in the first hundred years of the RCP8.5 simulation. After CO_2 stabilization, the land response ranges from strong emissions (Bern3D-LPJ) to weak uptake (UVic) under all RCPs (not shown). RCP differences in land carbon uptake during the 21st century result from different strengths of carbon cycle feedbacks, but also differences in land cover change. For instance, RCPs 4.5 and 6.0 include reforestation, while RCPs 2.6 and 8.5 assume substantial deforestation.

The behavior of land carbon uptake at 3000 as a function of atmospheric CO_2 varies strongly across models: while some EMICs simulate an increase in land uptake with in-

creasing CO_2 (e.g. DCESS), others simulate a strong decrease (Bern3D-LPJ) (Fig. 5c). Bern3D-LPJ has the highest sensitivity of land carbon uptake to temperature (Eby et al. 2013), as it includes a representation of carbon release from permafrost soils and peatlands. The land uptake fraction increases from RCP2.6 to RCP4.5 in most models, and remains approximately constant or decreases from RCP4.5 to RCP8.5 (the ensemble mean land uptake fraction remains approximately constant across RCPs). The low land uptake fraction under RCP2.6 in some models may be due to relatively large LUC emissions (Arora et al. 2011).

Our results differ from those of a previous EMIC intercomparison (Plattner et al. 2008), which found that the fractional distribution of excess carbon among the atmosphere, ocean and terrestrial biosphere remained approximately constant across scenarios. That study, however, considered a much narrower range in atmospheric CO_2 changes ($\sim$700–1000 PgC).

c. Pre-industrial CO_2 emission commitment

Pre-industrial CO_2 emission commitment (PIEM-CO_2) is investigated by setting the anthropogenic CO_2 emission perturbation to zero after 2300 and letting the atmospheric CO_2 concentration evolve freely. Non-CO_2 radiative forcing is held constant at year-2300 levels. These simulations were performed by EMICs with an interactive carbon cycle only. As discussed in section 2b, setting the anthropogenic perturbation to zero does not result in zero emissions exactly: decadal-mean CO_2 emissions after 2300 range from -0.5 $PgCyr^{-1}$ to 0.5 $PgCyr^{-1}$ for all RCPs (Fig. 6). CO_2 emissions are ≤ 0 in all models, except for the UMD model. The long-term effect of these annual emissions is evident in Fig. 7 for the RCP2.6 PIEM-CO_2 commitment simulation, with cumulative emissions declining between 2300 and 3000 (with exception of the UMD model, for which cumulative emissions increase). Note that despite the slightly different model setup, the PIEM-CO_2 commitment simulations are comparable to the zero-CO_2-emission commitment simulations discussed in the literature.

As CO_2 emissions nearly cease, atmospheric CO_2 declines as the ocean and land continue

to absorb carbon from the atmosphere (Fig. 6). The efficacy of carbon uptake differs between models, and so does the rate of decline of atmospheric CO_2. By the year 3000, atmospheric CO_2 is still far away from a new equilibrium due to the long timescales of CO_2 removal from the atmosphere (Eby et al. 2009). By 3000, the ensemble mean atmospheric CO_2 is 330 ppmv in RCP2.6, 440 ppmv in RCP4.5, 590 ppmv in RCP6.0 and 1560 ppmv in RCP8.5. Note that the upper boundary of the atmospheric CO_2 range spanned by models increases after 2300. The upper limit is set by the UMD model, which has slightly positive CO_2 emissions. Atmospheric CO_2 at 3000 in RCPs 4.5–8.5 is still at a high fraction (≥ 0.5) of the peak atmospheric CO_2 in all models (Fig. 8). These results are consistent with previous studies (Montenegro et al. 2007; Archer and Brovkin 2008; Plattner et al. 2008; Eby et al. 2009; Solomon et al. 2009; Archer et al. 2009), which showed that a significant fraction of CO_2 remains airborne after several hundred years, and that this fraction increases with higher CO_2 concentrations (or emissions).

Despite decreasing radiative forcing after 2300 in most models, global mean temperature decreases only slightly in RCPs 4.5–6.0 between 2300 and 3000 and remains approximately constant in RCP8.5 (Table 4). This near constancy of global mean temperature after elimination of anthropogenic CO_2 emissions is known from earlier studies with EMICs and complex Earth System models (Matthews and Caldeira 2008; Plattner et al. 2008; Eby et al. 2009; Solomon et al. 2009; Lowe et al. 2009; Froelicher and Joos 2010; Gillett et al. 2011; Zickfeld et al. 2012) and results from the cancellation of two opposing effects: the delayed warming due to ocean thermal inertia and the decrease in radiative forcing associated with declining atmospheric CO_2 levels in conjunction with the logarithmic dependence of forcing on atmospheric CO_2 (Eby et al. 2009; Solomon et al. 2010). At 3000, the fraction of warming that persists relative to that in the year 2300 (the year the anthropogenic perturbation is set to zero, which approximately corresponds to the year of peak warming) is 0.85, 0.89 and 0.99 in the ensemble mean for RCPs 4.5, 6.0 and 8.5 respectively (Fig. 8). These values are consistent with those from Eby et al. (2009), who found that 80–100% of the warming

anomaly persists 700 years after emissions were eliminated, with the fraction increasing with the amount of cumulative emissions.

In contrast to global mean temperature, sea level rise due to thermal expansion continues after elimination of anthropogenic CO_2 emissions in RCPs 4.5–8.5. The sea level rise between 2300 and 3000 is substantial in these scenarios (Table 4) and comparable to the sea level rise between 1850 and 2300. While sea level rise in some EMICs levels off toward the end of the simulation, it continues to rise in others. This is consistent with the results of a previous EMIC intercomparison (Plattner et al. 2008). In zero-emission commitment simulations with a complex Earth System Model, Gillett et al. (2011) found thermosteric sea level to still rise 900 years after cessation of emissions. Given that surface air temperature remains elevated for centuries to millennia and intermediate-depth temperature in the high latitude Southern Ocean continues to warm, potentially leading to a collapse of the West Antarctic ice sheet (Gillett et al. 2011), thermal expansion on these timescales is likely to be compounded by large sea level contributions from disintegrating ice sheets.

Both global mean warming and sea level rise behave differently in RCP2.6 than in the higher scenarios (Fig. 7). Due to the strong decline in atmospheric CO_2 and, accordingly, radiative forcing already before 2300, the warming and sea level rise commitment after 2300 are lower in this scenario. Global mean temperature continues to decrease between 2300 and 3000 and sea level stabilizes or even starts to slightly drop in some models (except for the UMD model, for which atmospheric CO_2 increases after 2300).

An interesting question in view of the comparability of results from different studies is whether the pre-industrial (or zero) CO_2 emission commitment is dependent on the time CO_2 emissions cease. We address this question by comparing the temperature and thermal expansion commitment in PIEM-CO_2 simulations with those in the reversibility simulations (REc) with constant year-2300 radiative forcing to the year 3000 and zero CO_2 emissions thereafter. If CO_2 emissions cease earlier (e.g. in 2300 as opposed to 3000) the system is further away from equilibrium with the stabilized radiative forcing, the fraction of realized

warming is smaller (Fig. 2b), and one would expect a larger temperature and thermal expansion commitment. One complicating factor in our comparison is that the PIEM-CO_2 simulations entail slightly negative (as opposed to zero) emissions in most models, leading to a more rapid decline in atmospheric CO_2 and hence radiative forcing after cessation of emissions. The model average decrease in surface air temperature after emissions cease is lower in the REc than in the PIEM-CO_2 simulations (-0.2°C versus -0.5°C for RCPs 4.5 and 6.0), which we attribute to the slower decline in radiative forcing in the REc simulations. On the other hand, the thermal expansion commitment is larger in the PIEM-CO_2 simulations (0.3 m versus 0.1 m in the REc simulation for RCP 6.0), consistent with the smaller fraction of realized warming at the time emissions cease. These results indicate that the temperature commitment is determined largely by the radiative forcing after emissions cease, whereas the thermal expansion commitment is determined by the radiative forcing before emissions cease, consistent with the longer response timescale of the deep ocean.

d. Pre-industrial emission commitment

The pre-industrial emission commitment simulations (PIEM) are similar to the PIEM-CO_2 simulations described in the previous paragraph, except that non-CO_2 radiative forcing is abruptly set to zero in the year 2300. Note that this is different from setting emissions of non-CO_2 gases to zero because the finite atmospheric lifetime of these gases would lead to a gradual decline in their concentration and associated radiative forcing (except for aerosols, which have a very short atmospheric residence time). Similar to the PIEM-CO_2 runs, atmospheric CO_2 declines after 2300 under all RCPs (Fig. 9). The rate of decrease is slightly larger than in the PIEM-CO_2 simulations due to the greater efficiency of the carbon sinks in a slightly cooler climate (i.e. a reduced climate-carbon cycle feedback). The surface temperature decreases abruptly around 2300, and more gradually thereafter, with a rate similar to that in the PIEM-CO_2 simulations. Accordingly, the warming commitment after 2300 is more negative than in the PIEM-CO_2 runs (Table 4). Note that the temperature response

in the simulations described here is different from that projected in simulations where all anthropogenic emissions are set to zero (Hare and Meinshausen 2006; Armour and Roe 2011; Matthews and Zickfeld 2012). In those simulations, temperature increases temporarily after elimination of emissions due to the removal of the negative radiative forcing from aerosols (Hare and Meinshausen 2006; Armour and Roe 2011; Matthews and Zickfeld 2012). In the RCPs used in the present study, the year-2300 non-CO_2 radiative forcing is dominated by the positive forcing from non-CO_2 greenhouse gases such that a removal of this forcing leads to a sudden cooling.

The sea level rise commitment in PIEM simulations is smaller than in PIEM-CO_2 simulations (Table 4), consistent with the more rapid decline in radiative forcing .

e. Constant emission commitment

The constant emission commitment simulations (CEM) differ from the simulations described previously in that CO_2 emissions are held constant at significant positive values after 2300 in RCPs 4.5–8.5 (range of 0.8–6.4 $PgCyr^{-1}$; Fig. 10). Since only a fraction of these CO_2 emissions is taken up by carbon sinks, atmospheric CO_2 increases again after 2300 (as opposed to remaining constant or decreasing as in the other commitment simulations). As a result, surface air temperature continues to increase, with a significant positive warming commitment after 2300 (Table 4). Thermosteric sea level also continues to rise after 2300, with the sea level rise between 2300 and 3000 being several factors larger than that realized by 2300 (Table 4).

The climate response in the RCP2.6 CEM simulation is very different from that under the higher RCPs: CO_2 emissions in the year 2300 are slightly negative in all models (-0.7 to -0.2 $PgCyr^{-1}$), and holding emissions fixed at these values results in a continuing decrease in atmospheric CO_2. Accordingly, global mean temperature continues to decrease, and sea level starts to fall between 2300 and 3000 in all models. The ensemble mean warming and sea level rise commitments are slightly more negative than to those in the RCP2.6 PIEM

commitment simulations (Table 4).

f. Climate change reversibility

To explore under which conditions the climate system can revert to its pre-industrial state, a set of "reversibility" simulations was carried out. These simulations were started from the year-3000 state of the constant composition commitment (CCO) simulations. Two simulations were performed with atmospheric CO_2 decreasing linearly to zero ("ramp") over a period of 100 and 1000 years, respectively. These scenarios are highly idealized and are used for illustrative purpose only. Since the atmospheric CO_2 changes are externally prescribed, these simulations give insight into the reversibility of the physical climate system. A third simulation, in which atmospheric CO_2 is allowed to evolve freely after emissions are set to zero, is aimed at exploring the reversibility of changes in the coupled climate-carbon cycle system. It should be noted that non-CO_2 forcing after year 3000 is held fixed at slightly positive values and therefore the total forcing after ramp-down of atmospheric CO_2 to pre-industrial levels is different from zero.

With atmospheric CO_2 decreasing to pre-industrial levels over a period of 100 years, surface air temperature decreases rapidly at first (during the CO_2 ramp-down phase) and more slowly thereafter (Fig. 11). At the year 4000 surface air temperature is still higher than under 1851–1860 conditions (Table 5). This remaining warming 900 years after atmospheric CO_2 returned to pre-industrial levels can be explained by the thermal inertia of the climate system, which plays out both during periods of warming and cooling, and the (small) residual positive radiative forcing from non-CO_2 sources.

The thermosteric sea level rise trend is also reversed with decreasing atmospheric CO_2. Rates of sea level fall, however, are slower than rates of cooling, and sea level is significantly higher than under pre-industrial conditions at year 4000 (Table 5). The thermohaline circulation exhibits a rapid strengthening in the ensemble mean during the CO_2 decrease phase, with the overturning first overshooting and then slowly converging to pre-industrial values.

Note that under RCP8.5 the thermohaline circulation is close to collapse in the Bern3D-LPJ model, but recovers after the ramp-down of atmospheric CO_2.

In the simulations with a slower decrease of atmospheric CO_2 (over 1000 years), surface air temperature also starts to drop after the year 3000, but the cooling is more gradual than in the 100-year ramp-down experiment (Fig. 12). Also, the rate of cooling is lower during the first 500 years of the ramp-down than during the last 500 years. This nonlinear response can again be explained with the thermal inertia of the climate system: despite 700 years of constant forcing (from 2300 to 3000) the climate system is still equilibrating with that forcing, and the associated warming commitment acts to offset the cooling due to decreasing CO_2 levels during the first few hundred years of the CO_2 ramp-down phase. Surface air temperature at 4000 is warmer than in the simulations with a 100-year ramp-down, particularly for the higher RCPs (Table 5).

In contrast to temperature, thermosteric sea level continues to rise for several centuries after CO_2 starts to decrease. For instance, ensemble mean sea level does not peak until the year 3200 under RCP6.0 and 3300 under RCP8.5. Year-4000 sea level rise is twice as high in these simulations than in the 100-year ramp-down experiments (Table 5). The thermohaline circulation recovers slowly at first and more rapidly towards the end of the CO_2 decrease phase. Under RCPs 4.5–8.5 the ensemble-mean overturning at year 4000 exceeds the pre-industrial value. Individual models deviate substantially from the ensemble-mean behavior. For instance, overturning in the Bern3D-LPJ model does not recover under declining CO_2 levels, but collapses completely around the year 3500.

In the third reversibility experiment, atmospheric CO_2 is allowed to evolve freely after the year 3000 (under zero CO_2 emissions). This simulation was performed by a subset of EMICs with an interactive carbon cycle only. It is similar to the pre-industrial CO_2-emission commitment (PIEM-CO_2) simulation, except that a 700-year CO_2 stabilization phase precedes the free-evolving-CO_2 phase (and emissions are exactly zero as opposed to slightly negative in the PIEM-CO_2 experiments). Following the cessation of CO_2 emissions, atmospheric CO_2

declines due to CO_2 uptake by marine and terrestrial carbon sinks (Fig. 13). As discussed earlier for the PIEM-CO_2 experiments, surface air temperature remains approximately constant after elimination of CO_2 emissions, while sea level continues to rise. Compared to the reversibility experiments with CO_2 ramp-down, surface air temperature and sea level rise at 4000 are much higher in the free-evolving-CO_2 case (Table 5). Similarly to surface air temperature, the thermohaline circulation remains approximately constant after emissions cease. An exception is again the overturning in the Bern3D-LPJ model, which collapses completely by the year 3200.

EMICs with an interactive carbon cycle were used to diagnose the CO_2 emissions compatible with the CO_2 concentration trajectories for the two reversibility experiments with CO_2 ramp-down (Fig. 14). The abrupt decrease of atmospheric CO_2 in the two experiments (Figs. 11a, 12a) requires emissions to become negative to close the CO_2 budget. Emissions are much more negative in the experiments with a fast (100-year) ramp-down than in those with a slower (1000-year) ramp-down, particularly under the higher RCPs. For each experiment, the larger the rate of atmospheric CO_2 decline, the more negative the diagnosed CO_2 emissions.

Negative emissions imply that the prescribed rate of atmospheric CO_2 decline exceeds the uptake capacity of the marine and terrestrial carbon sinks. In the 100-year ramp-down experiments, terrestrial carbon inventories decline strongly during the CO_2 decrease phase, and remain relatively stable thereafter in all models (Fig. 15). At year 4000, terrestrial carbon inventories are lower than at pre-industrial. The likely reason is the lag of surface air temperature relative to atmospheric CO_2, such that the terrestrial biosphere is subject to higher temperatures despite a return to pre-industrial CO_2 conditions. Ocean carbon inventories also decline during the CO_2 ramp-down phase, although more gradually, and continue to decline until the end of the simulation in all models. At year 4000, ocean carbon inventories are higher than at pre-industrial in most models.

In the 1000-year ramp-down experiment, the decline in land carbon inventories in re-

sponse to declining CO_2 levels is more gradual and continues for the duration of the ramp-down (not shown). Ocean carbon inventories, on the other hand, continue to increase after the decline in atmospheric CO_2 in several models (exceptions are the UVic and UMD models). By year 3500, ocean carbon turns around and starts to decrease in all models. Continuing ocean carbon uptake at the beginning of the ramp-down phase offsets the carbon release from the terrestrial biosphere at first, such that diagnosed CO_2 emissions are only slightly negative. Diagnosed emissions become increasingly more negative towards the end of the ramp-down as both ocean and land release CO_2 into the atmosphere (Fig. 14b).

g. Cumulative emissions compatible with temperature targets

A last set of simulations was performed with the the UVic and Bern3D-LPJ EMICs to explore the cumulative emissions compatible with long-term temperature targets. These simulations used an inverse modelling approach, whereby CO_2 emissions compatible with prescribed temperature trajectories were diagnosed (Zickfeld et al. 2009). Fig. 16 displays the diagnosed cumulative emissions for temperature trajectories stabilizing at 1.5°C, 2°C, 3°C and 4°C for the UVic and Bern3D-LPJ EMICs. The temperature trajectories prescribed to the two models are slightly different until the time of temperature stabilization (Fig. 16a). This does not affect the comparability of results, however, since we discuss the cumulative emissions since pre-industrial, and the climate response centuries after elimination of emissions is independent of the emission trajectory (Eby et al. 2009; Zickfeld et al. 2009, 2012). Model mean allowable cumulative emissions are 770 PgC, 1000 PgC, 1460 PgC and 1950 PgC for temperature targets of 1.5°C, 2°C, 3°C and 4°C, respectively. These estimates are slightly lower than the allowable cumulative emissions estimated with an earlier version of the UVic model (Zickfeld et al. 2009). The estimate for the 2°C target coincides with the value of 1000 PgC from Allen et al. (2009), and is somewhat higher than the value calculated by Meinshausen et al. (2009), who assumed stronger forcing from non-CO_2 gases.

Allowable cumulative emissions at 2500 are slightly higher in the Bern3D-LPJ than in

the UVic model for the lower temperature targets (1.5–2°C), whereas they are lower for the highest temperature target (4°C). Allowable emissions consistent with temperature targets depend both on the physical and biogeochemical model response. For instance, the higher the climate sensitivity and/or the stronger the (positive) climate-carbon cycle feedback, the lower the amount of cumulative emissions consistent with a specified temperature target (Zickfeld et al. 2009). Both EMICs have a relatively high climate sensitivity and a high total carbon uptake sensitivity to temperature, but also a high total carbon uptake sensitivity to CO_2 (Eby et al. 2013, Tables 2, 4). The relative ordering of these sensitivities between the two models is time and scenario dependent (e.g. the equilibrium climate sensitivity is higher in UVic than Bern3D-LPJ at $2\times CO_2$, but lower at $4\times CO_2$) which may explain the change in ordering of allowable emissions with the level of temperature stabilization.

Matthews et al. (2009) proposed the Climate Carbon Response (CCR), defined as the ratio of temperature change to cumulative carbon emissions, as a metric for the combined physical and biogeochemical response of the climate system to CO_2 emissions. CCR has been suggested to be relatively insensitive to the emissions scenario, and approximately constant over time. Eby et al. (2013) calculated the CCR for eight EMICs with an interactive carbon cycle from an idealized $4\times CO_2$ experiment with a 1% CO_2 increase per year and noted that the CCR in the EMICS varies appreciably with time. At the time of CO_2 doubling, the CCR ranges from 1.4°C EgC^{-1} to 2.5°C EgC^{-1} (note that these numbers differ from those in Table 4 of Eby et al. (2013), which are taken at the time of CO_2 quadrupling). The models' CCR can be inverted to compute the range of cumulative emissions consistent with temperature targets. Ensemble mean allowable cumulative emissions are 830 PgC, 1100 PgC, 1650 PgC and 2200 PgC for temperature targets of 1.5°C, 2°C, 3°C and 4°C, respectively (Fig. 17). Since the CCR was computed for cumulative emissions of about 1000 PgC, CCR-based allowable emission estimates for temperature targets of 1.5–2°C are likely more accurate than those for the higher temperature targets. While the cumulative emissions estimated from the temperature tracking experiments and the CCR are very simi-

lar for the Bern3D-LPJ model, particularly for lower temperature targets, the CCR-derived estimates are considerably higher for the UVic model. The difference in the UVic model's allowable emissions estimates for the low temperature targets could be explained by a net positive radiative forcing from non-CO_2 sources in the temperature tracking simulations (not present in the idealized $4\times CO_2$ simulation from which the CCR was derived), which reduces the amount of allowable CO_2 emissions. Due to differences in forcing implementation, the non-CO_2 radiative forcing imbalance seems not to be present in the Bern3D-LPJ temperature tracking runs, such that the two allowable emissions estimates are very similar for low temperature targets. For higher targets, the discrepancy between the CCR-based and temperature-tracking-derived estimates is likely due to the time and scenario dependence of CCR.

4. Summary and Conclusions

We presented results from long-term climate projections with twelve EMICs. The first set of projections are climate change commitment simulations run until the year 3000. Three different types of climate commitment are considered: (i) constant composition, (ii) pre-industrial emission, and (iii) constant emission commitments. All commitment simulations follow common CO_2 concentration trajectories until the year 2300 - the four RCP scenarios (2.6, 4.5, 6.0 and 8.5) and their extensions. Climate projections to 2300 are consistent with results from AOGCMs, confirming that EMICs are well suited to complement simulations with more complex models. Simulated ensemble-mean surface air temperatures exceed the 2°C target set by the Copenhagen Accord in all scenarios, except for the low emissions RCP2.6 scenario. Under this scenario, the model ensemble mean temperature peaks at 1.7°C relative to pre-industrial, and returns to 1.3°C by 2300. The spread between models, however, is considerable, and peak warming in a few models exceeds the 2°C target.

EMICs simulate substantial surface air temperature and thermosteric sea level rise com-

mitment following stabilization of the atmospheric composition at year-2300 levels for RCPs 4.5, 6.0 and 8.5. For these scenarios, the thermosteric sea level rise between years 2300 and 3000 amounts to several times the sea level rise by the time of radiative forcing stabilization. Sea level rise due to thermal expansion still continues at the year 3000 under all scenarios considered. The Atlantic meridional overturning circulation is weakened temporarily under RCPs 2.6–6.0 and recovers to within 80% of the pre-industrial value several centuries after forcing stabilization. The MOC weakening is more persistent for RCP8.5, with one model close to a complete collapse in the year 3000.

EMICs with an interactive carbon cycle are used to diagnose the CO_2 emissions compatible with the CO_2 concentration pathways specified for the constant composition commitment simulations. Diagnosed cumulative emissions between 1850 and 3000 increase approximately linearly with atmospheric CO_2 for RCPs 2.6–6.0, but the increase becomes less than linear at higher radiative forcing. The year-3000 airborne fraction of cumulative emissions increases with increasing atmospheric CO_2. The increasing airborne fraction is due largely to a decrease in the ocean uptake fraction with higher radiative forcing. The model ensemble mean land uptake fraction is rather constant across RCP scenarios, but the CO_2 dependence varies strongly between models.

Elimination of anthropogenic CO_2 emissions after 2300 and constant year-2300 non-CO_2 radiative forcing results in slowly decreasing atmospheric CO_2 concentrations. At year 3000 atmospheric CO_2 is still at more than half the year-2300 level in all EMICs for RCPs 4.5–8.5, with the fraction increasing with RCP scenario. Surface air temperature remains nearly constant or decreases slightly in all EMICs, with 85–99% of the maximum warming still persisting in the year 3000 for RCPs 4.5–8.5. Sea level rise due to thermal expansion continues after elimination of CO_2 emissions in RCPs 4.5–8.5 and is comparable to the sea level rise between 1850 and 2300. At 3000, 700 years after anthropogenic CO_2 emissions are zeroed, sea level is still rising in several EMICs. If radiative forcing from non-CO_2 forcing agents is eliminated simultaneously with CO_2 emissions, the warming and thermosteric sea

level rise are slightly lower than in the simulations with elimination of CO_2 emissions alone, but still remain substantially higher in the year 3000 compared to pre-industrial.

The largest warming and thermosteric sea level rise commitment are simulated for the case with CO_2 emissions held fixed at year-2300 levels and constant year-2300 non-CO_2 radiative forcing. In response to anew increasing atmospheric CO_2 levels after 2300, surface air temperature and sea level continue to rise, with a substantial post-2300 commitment.

The climate change commitment associated with the low emissions scenario RCP 2.6 differs from that of the higher RCPs. Due to the decline in atmospheric CO_2 and radiative forcing already before 2300, the warming and thermosteric sea level rise commitment after 2300 are lower in this scenario. The difference is largest for the constant emissions commitment simulations, since year-2300 emissions are negative (as opposed to positive in the other scenarios). Accordingly, atmospheric CO_2 decreases after 2300, surface air temperature continues to cool, and sea level starts to fall.

Results of the climate change commitment simulations differ widely between EMICs, both in the physical and biogeochemical response. The difference in the response of the terrestrial carbon cycle to atmospheric CO_2 and climate is particularly large. Compared to an earlier EMIC intercomparison (Plattner et al. 2008), the range of carbon cycle responses appears to have even widened. This may be explained by the larger number of coupled climate-carbon cycle models included in the present model intercomparison, and the increase in model complexity since the Plattner et al. (2008) study. Most EMICs now include interactive representation of land use change emissions. One model includes representation of carbon release from permafrost and peatlands, while another includes nitrogen limitation. On the ocean side, several models now include representation of sediment processes. The large model spread suggests that continued efforts are needed to better understand the processes driving the response of land and ocean uptake to CO_2 and climate, and to better represent these processes in models.

If CO_2 emissions cease, and it is left to the natural carbon sinks to take up excess

CO_2, atmospheric CO_2 declines only slowly, and climate change is largely irreversible on centennial to millennial timescales, as discussed above in the context of the pre-industrial emission commitment simulations. Two additional experiments were carried out by EMICs to explore the reversibility of the climate system in response to an artificial "ramp-down" of atmospheric CO_2 to pre-industrial levels (over 100 and 1000 years). Due to the large thermal inertia of the ocean, surface air temperature and sea level rise exhibit a substantial time lag relative to atmospheric CO_2. 900 years after CO_2 is restored to pre-industrial levels, surface air temperature and particularly sea level are still considerably higher than under 1851–1860 conditions. The thermohaline circulation strengthens rapidly during the CO_2 decrease phase, first overshooting and then slowly converging to the pre-industrial value. If atmospheric CO_2 is returned to pre-industrial levels more slowly (over 1000 years), surface air temperature also cools more slowly, and sea level continues to rise for several centuries before starting to fall. The model ensemble mean thermohaline circulation recovers slowly at first and more rapidly towards the end of the CO_2 decrease phase. The ramp-down of CO_2 to pre-industrial levels over 100–1000 years requires large negative emissions, i.e. net removal of CO_2 drom the atmosphere, which are likely unrealistic with technologies currently available to capture CO_2 from the atmosphere (McGlashan et al. 2012).

In summary, results from the commitment and reversibility simulations suggest that it is very difficult to revert from a given level of warming on timescales relevant to human activities, even after complete elimination of emissions. Reversing global warming may be desirable if climate change exceeds adaptive capacities of natural and human systems. Our results suggest that significant negative emissions have the potential to reverse global warming but whether CO_2 capture technology is feasible at the necessary scale is debatable.

Using an inverse modelling approach, two EMICs (Bern3D-LPJ, UVic) estimated the cumulative CO_2 emissions ("CO_2 budget") compatible with long-term global mean temperature stabilization targets. Cumulative emissions between pre-industrial and the year 2500 are similar between the two models and amount to a mean value of 1000 PgC for the 2°C.

A somewhat higher model ensemble mean estimate is derived based on the Climate Carbon Response (CCR; Matthews et al. (2009)) computed for EMICs with an interactive carbon cycle. As cumulative CO_2 emissions from fossil fuels and land use up to today amount to about 500 PgC, the remaining CO_2 budget consistent with the 2°C target is about 500 PgC, assuming that the radiative forcing of non-CO_2 greenhouse gases continues to be compensated by negative aerosol forcing, as has been approximately the case in the past. The results of this model intercomparison therefore support the conclusions from previous studies that it is still possible in theory to meet the 2°C target, but leeway is getting tight, particularly in the face of socio-economic and technological inertia.

Acknowledgments.

KZ and AJW acknowledge support from the National Science and Engineering Research Council (NSERC) Discovery Grant Program. AJW acknowledges support from NSERC's G8 Research Councils Initiative on Multilateral Research Funding Program. AVE and IIM were supported by the the President of Russia grant 5467.2012.5, by the Russian Foundation for Basic Research, and by the programs of the Russian Academy of Sciences. EC, TF, HG and GPB acknowledge support from the Belgian Federal Science Policy Office. FJ, RS and MS acknowledges support by the Swiss National Science Foundation and by the European Project CARBOCHANGE (grant 264879) which received funding from the European Commissions Seventh Framework Programme (FP7/20072013). PBH and NRE acknowledge support from EU FP7 grant ERMITAGE no. 265170.

REFERENCES

Allen, M. R., D. J. Frame, C. Huntingford, C. D. Jones, J. A. Lowe, M. Meinshausen, and N. Meinshausen, 2009: Warming caused by cumulative carbon emissions towards the trillionth tonne. *Nature*, **458**, 1163–1166.

Archer, D. and V. Brovkin, 2008: The millennial atmospheric lifetime of anthropogenic CO_2. *Clim. Change*, **90 (3)**, 283–297, doi:10.1007/s10584-008-9413-1.

Archer, D., et al., 2009: Atmospheric Lifetime of Fossil Fuel Carbon Dioxide. *Annu. Rev. Earth Planet. Sci.*, **37**, 117–134, doi:10.1146/annurev.earth.031208.100206.

Armour, K. C. and G. H. Roe, 2011: Climate commitment in an uncertain world. *Geophys. Res. Lett.*, **38**, doi:10.1029/2010GL045850.

Arora, V. K., J. F. Scinocca, G. J. Boer, J. R. Christian, K. L. D. G. M. Flato, V. V. Kharin, W. G. Lee, and W. J. Merryfield, 2011: Carbon emission limits required to satisfy future representative concentration pathways of greenhouse gases. *Geophys. Res. Lett.*, **38**, L05 805, doi:10.1029/2010GL046270.

Azar, C., K. Lindgren, E. Larson, and K. Möllersten, 2006: Carbon Capture and Storage From Fossil Fuels and Biomass Costs and Potential Role in Stabilizing the Atmosphere. *Clim. Change*, **47**, 47–79.

Boucher, O., et al., 2012: Reversibility in an earth system model in response to CO_2 concentration changes. *Env. Res. Lett.*, **7**, doi:10.1088/1748-9326/7/2/024013.

Church, J. A., et al., 2013: Sea Level Change. *Climate Change 2013: The Physical Science Basis, Contribution of WG I to the Fourth Assessment Report of the IPCC*, T. Stocker

and D. Qin, Eds., Cambridge University Press, Cambridge, UK and New York, USA, In Preparation.

Collins, M., et al., 2013: Long-term Climate Change: Projections, Commitments and Irreversibility. *Climate Change 2013: The Physical Science Basis, Contribution of WG I to the Fourth Assessment Report of the IPCC*, T. Stocker and D. Qin, Eds., Cambridge University Press, Cambridge, UK and New York, USA, In Preparation.

Denman, K. L., et al., 2007: Coupling between changes in the climate system and biogeochemistry. *Climate Change 2007: The Physical Science Basis, Contribution of WG I to the Fourth Assessment Report of the IPCC*, S. Solomon, D. Qin, and M. Manning, Eds., Cambridge University Press, Cambridge, UK and New York, USA, 499–587.

Eby, M., K. Zickfeld, A. Montenegro, D. Archer, K. J. Meissner, and A. J. Weaver, 2009: Lifetime of anthropogenic climate change: millennial time scales of potential CO_2 and temperature perturbations. *J. Clim.*, **22**, 2501–2511.

Eby, M., et al., 2013: Historical and idealized climate model experiments: An EMIC intercomparison. *Climate of the Past*, in revision.

Eliseev, A. V. and I. I. Mokhov, 2011: Uncertainty of climate response to natural and anthropogenic forcings due to different land use scenarios. *Adv. Atmos. Sci.*, **28 (5)**, 1215–1232, doi:10.1007/s00376-010-0054-8.

Friedlingstein, P., et al., 2006: Climate-carbon cycle feedback analysis: Results from the C4MIP model intercomparison. *J. Clim.*, **19**, 3337–3353.

Froelicher, T. and F. Joos, 2010: Reversible and irreversible impacts of greenhouse gas emissions in multi-century projections with a comprehensive climate-carbon model. *Clim. Dyn.*, **35 (7–8)**, 1439–1459, doi:10.1007/s00382-009-0727-0.

GEA, 2012: *Global Energy Assessment- Toward a Sustainable Future*. Cambridge University Press, Cambridge, UK and New York, NY, USA and the International Institute for Applied Systems Analysis, Laxenburg, Austria.

Gillett, N., V. Arora, K. Zickfeld, S. Marshall, and W. Merryfield, 2011: Ongoing climate change following a complete cessation of carbon dioxide emissions. *Nat. Geosci.*, **4**, 83–87.

Goosse, H., et al., 2010: Description of the Earth system model of intermediate complexity LOVECLIM version 1.2. *Geosci. Model Dev.*, **3 (2)**, 603–633, doi:10.5194/gmd-3-603-2010.

Hansen, J., G. Russell, A. Lacis, I. Fung, D. Rind, and P. Stone, 1985: Climate response-times - dependence on climate sensitivity and ocean mixing. *Science*, **229 (4716)**, 857–859, doi:10.1126/science.229.4716.857.

Hare, B. and M. Meinshausen, 2006: How much warming are we committed to and how much can be avoided? *Clim. Change*, **75 (1-2)**, 111–149, doi:10.1007/s10584-005-9027-9.

Held, I. M., M. Winton, K. Takahashi, T. Delworth, F. Zeng, and G. K. Vallis, 2010: Probing the Fast and Slow Components of Global Warming by Returning Abruptly to Preindustrial Forcing. *J. Clim.*, **23 (9)**, 2418–2427, doi:10.1175/2009JCLI3466.1.

Holden, P. B., N. R. Edwards, D. Gerten, and S. Schaphoff, 2013: A model based constraint on CO_2 fertilisation. *Biogeosci.*, **10**, 339–355, doi:10.5194/bg-10-339-2013.

Keith, D., M. Ha-Duong, and J. Stolaroff, 2006: Climate strategy with CO_2 capture from the air. *Clim. Change*, **74 (1-3)**, 17–45, doi:10.1007/s10584-005-9026-x.

Lowe, J. A., C. Huntingford, S. C. B. Raper, C. D. Jones, S. K. Liddicoat, and L. K. Gohar, 2009: How difficult is it to recover from dangerous levels of global warming? *Environ. Res. Lett.*, **4 (1)**, doi:10.1088/1748-9326/4/1/014012.

MacDougall, A., C. Avis, and A. Weaver, 2012: Significant existing commitment to warming from the permafrost carbon feedback. *Nat. Geosc.*, **5**, 719–721.

Matsumoto, K., K. S. Tokos, A. R. Price, and S. J. Cox, 2008: First description of the Minnesota Earth System Model for Ocean biogeochemistry (MESMO 1.0). *Geosci. Model Dev.*, **1 (1)**, 1–15.

Matthews, H. D. and K. Caldeira, 2008: Stabilizing climate requires near-zero emissions. *Geophys. Res. Lett.*, **35 (4)**, L04 705, doi:10.1029/2007GL032 388.

Matthews, H. D., N. P. Gillett, P. A. Stott, and K. Zickfeld, 2009: The proportionality of global warming to cumulative carbon emissions. *Nature*, **459**, 829–832.

Matthews, H. D. and A. J. Weaver, 2010: Committed climate warming. *Nat. Geosci.*, **3 (3)**, 142–143, doi:10.1038/ngeo813.

Matthews, H. D. and K. Zickfeld, 2012: Climate response to zeroed emissions of greenhouse gases and aerosols. *Nat. Clim. Chang.*, **2 (5)**, 338–341, doi:10.1038/NCLIMATE1424.

McGlashan, N., N. Shah, B. Caldecott, and M. Workman, 2012: High-level techno-economic assessment of negative emissions technologies. *Process Safety and Environmental Protection*, **90**, 501–510.

Meehl, G., W. Washington, W. Collins, J. Arblaster, A. Hu, L. Buja, W. Strand, and H. Teng, 2005: How much more global warming and sea level rise? *Science*, **307 (5716)**, 1769–1772, doi:10.1126/science.1106663.

Meehl, G., et al., 2007: Global climate projections. *Climate Change 2007: The Physical Science Basis, Contribution of WG I to the Fourth Assessment Report of the IPCC*, S. Solomon, D. Qin, and M. Manning, Eds., Cambridge University Press, Cambridge, UK and New York, USA, 747–845.

Meinshausen, M., N. Meinshausen, W. Hare, S. C. B. Raper, K. Frieler, R. Knutti, D. Frame, and M. Allen, 2009: Greenhouse-gas emission targets for limiting global warming to 2°C. *Nature*, **458**, 1158–1162.

Meinshausen, M., S. C. B. Raper, and T. M. L. Wigley, 2011a: Emulating coupled atmosphere-ocean and carbon cycle models with a simpler model, MAGICC6-Part 1: Model description and calibration. *Atmos. Chem. Phys.*, **11 (4)**, 1417–1456, doi: 10.5194/acp-11-1417-2011.

Meinshausen, M., et al., 2011b: The RCP greenhouse gas concentrations and their extensions from 1765 to 2300. *Clim. Change*, **109 (1-2, SI)**, 213–241, doi:10.1007/s10584-011-0156-z.

Montenegro, A., V. Brovkin, M. Eby, D. E. Archer, and A. J. Weaver, 2007: Long term fate of anthropogenic carbon. *Geophys. Res. Lett.*, **34**, L19 703, doi:10.1029/2007GL031 018.

Montoya, M., A. Griesel, A. Levermann, J. Mignot, M. Hofmann, A. Ganopolski, and S. Rahmstorf, 2005: The earth system model of intermediate complexity CLIMBER-3 alpha. Part 1: description and performance for present-day conditions. *Clim. Dyn.*, **25 (2-3)**, 237–263, doi:10.1007/s00382-005-0044-1.

Morice, C. P., J. J. Kennedy, N. A. Rayner, and P. D. Jones, 2013: Quantifying uncertainties in global and regional temperature change using an ensemble of observational estimates: The hadcrut4 dataset. *J. Geophys. Res.*, doi:10.1029/2011JD017187, in press.

Moss, R. H., et al., 2010: The next generation of scenarios for climate change research and assessment. *Nature*, **463 (7282)**, 747–756, doi:{10.1038/nature08823}.

Nusbaumer, J. and K. Matsumoto, 2008: Climate and carbon cycle changes under the overshoot scenario. *Global and Planetary Change*, **62**, 164–172.

Petoukhov, V., A. Ganopolski, V. Brovkin, M. Claussen, A. Eliseev, C. Kubatzki, and S. Rahmstorf, 2000: CLIMBER-2: a climate system model of intermediate complexity.

Part I: model description and performance for present climate. *Clim. Dyn.*, **16 (1)**, 1–17, doi:10.1007/PL00007919.

Plattner, G.-K., et al., 2008: Long-term climate commitments projected with climate-carbon cycle models. *J. Clim.*, **21**, 2721–2751.

Rhein, M., et al., 2013: Observations: Ocean. *Climate Change 2013: The Physical Science Basis, Contribution of WG I to the Fourth Assessment Report of the IPCC*, T. Stocker and D. Qin, Eds., Cambridge University Press, Cambridge, UK and New York, USA, In Preparation.

Ritz, S. P., T. F. Stocker, and F. Joos, 2011: A Coupled Dynamical Ocean-Energy Balance Atmosphere Model for Paleoclimate Studies. *J. Clim.*, **24 (2)**, 349–375, doi: 10.1175/2010JCLI3351.1.

Sabine, C. L., et al., 2004: The oceanic sink for anthropogenic CO_2. *Science*, **305**, 367–371.

Shaffer, G., S. M. Olsen, and J. O. P. Pedersen, 2008: Presentation, calibration and validation of the low-order, DCESS Earth System Model (Version 1). *Geosci. Model Dev.*, **1 (1)**, 17–51.

Sokolov, A., et al., 2005: The MIT Integrated Global System Model (IGSM) Version 2: Model Description and Baseline Evaluation. Tech. rep., MIT.

Solomon, S., J. S. Daniel, T. J. Sanford, D. M. Murphy, G.-K. Plattner, R. Knutti, and P. Friedlingstein, 2010: Persistence of climate changes due to a range of greenhouse gases. *Proc. Natl. Acad. Sci. U. S. A.*, **107 (43)**, 18 354–18 359, doi:10.1073/pnas.1006282107.

Solomon, S., G.-K. Plattner, R. Knutti, and P. Friedlingstein, 2009: Irreversible climate change due to carbon dioxide emissions. *Proc. Natl. Acad. Sci. U. S. A.*, **106 (6)**, 1704–1709.

940 Stocker, B. D., K. Strassmann, and F. Joos, 2011: Sensitivity of holocene atmospheric CO2
941 and the modern carbon budget to early human land use: analyses with a process-based
942 model. *Biogeosci.*, **8**, 69–88.

943 Tachiiri, K., J. C. Hargreaves, J. D. Annan, A. Oka, A. Abe-Ouchi, and M. Kawamiya,
944 2010: Development of a system emulating the global carbon cycle in Earth system models.
945 *Geosci. Model Dev.*, **3 (2)**, 365–376, doi:10.5194/gmd-3-365-2010.

946 Taylor, K. E., R. J. Stouffer, and G. A. Meehl, 2008: A summary of the CMIP5 experiment
947 design. Tech. rep.

948 Tsutsui, J., Y. Yoshida, D.-H. Kim, H. Kibata, K. Nishizawa, N. Nakashiki, and K. Mu-
949 rayama, 2007: Long-term climate response to stabilized and overshoot anthropogenic
950 forcings beyond the twenty first century. *Clim. Dyn.*, **28**, 199–214.

951 Weaver, A. J., et al., 2001: The UVic Earth System Climate Model: Model description,
952 climatology, and applications to past, present and future climates. *Atmos.-Ocean*, **39**,
953 361–428.

954 Wigley, T., 2005: The climate change commitment. *Science*, **307 (5716)**, 1766–1769, doi:
955 10.1126/science.1103934.

956 Yoshida, Y., K. Maruyama, J. Tsutsui, N. Nakashiki, F. O. Bryan, M. Blackmon, B. A.
957 Boville, and R. D. Smith, 2005: Multi-century ensemble global warming projections using
958 the Community Climate System Model (CCSM3). *J. Earth Simulator*, **3**, 2–10.

959 Zeng, N., H. Qian, E. Munoz, and R. Iacono, 2004: How strong is carbon cycle-
960 climate feedback under global warming? *Geophys. Res. Lett.*, **31 (L20203)**, doi:
961 10.1007/s00376-010-0054-8.

962 Zickfeld, K., V. K. Arora, and N. P. Gillett, 2012: Is the climate response to carbon emissions
963 path dependent? *Geophys. Res. Lett.*, **39**, L05 703, doi:10.1029/2011GL050205.

964 Zickfeld, K., M. Eby, H. Matthews, and A. J. Weaver, 2009: Setting cumulative emissions
965 targets to reduce the risk of dangerous climate change. *Proc. Natl. Acad. Sci. U.S.A.*,
966 **106 (38)**, 16 129–16 134.

List of Tables

TABLE 1. Model experiments.

Label	Simulation	Timeframe	Forcing		# Models
			CO_2	Non-CO_2 GHGs	
HIST	Historical	1850–2005	CMIP5 concentration	CMIP5 forcing	12
RCP	RCPs and extensions	2006–2300	CMIP5 concentration	CMIP5 forcing	12
CCO	Const. composition commit.	2301–3000	Const. year-2300 conc.	Const. year-2300 forc.	12
PIEM-CO_2	PI CO_2 emission commit.	2301–3000	Const. 1840–1850 emissions	Const. year-2300 forc.	7
PIEM	PI emission commit.	2301–3000	Const. 1840–1850 emissions	Const. 1840–1850 forc.	7
CEM	Const. emission commit.	2301–3000	Const. 2290–2300 emissions	Const. year-2300 forc.	7
REa	Reversibility a	3001–4000	Lin. decrease in conc. for 100 yrs	Const. year-2300 forc.	11
REb	Reversibility b	3001–4000	Lin. decrease in conc. for 1000 yrs	Const. year-2300 forc.	11
REc	Reversibility c	3001–4000	Zero emissions	Const. year-2300 forc.	7
TTR	Temperature tracking	2005–2500	Diagnosed	Lin. decrease to zero by 2300	2

TABLE 2. Changes in climate and carbon cycle variables from EMIC historical simulations and observations. Shown are the warming over the 20th century (ΔT), the rate of thermosteric sea level rise averaged over 1971–2010 (SLR_{th}), the carbon fluxes averaged over 1990–1999 and cumulative fluxes from 1800 to 1994. $Land_{LUC}$ are land-use change fluxes from simulations with land-use forcing only (see Eby et al. (2013)). $Land_{RES}$ is the residual land flux, which is derived as the difference between the land flux from the historical simulation with all forcings and $Land_{LUC}$. Carbon fluxes are positive when directed into the atmosphere. Observations-based estimates are from Morice et al. (2013) for the 20th century warming, Rhein et al. (2013, Table 3.1) for 1971–2010 thermal expansion, Denman et al. (2007, Table 7.1) for the 1990s carbon fluxes and Sabine et al. (2004) for the cumulative carbon fluxes.

Model	ΔT	SLR_{th}	1990s carbon fluxes				Cumulative fluxes 1800–1994		
			$Land_{LUC}$	$Land_{RES}$	Ocean	Emissions	Land	Ocean	Emissions
	(°C)	(mm/yr)	(PgC/yr)	(PgC/yr)	(PgC/yr)	(PgC/yr)	(PgC)	(PgC)	(PgC)
Bern3D-LPJ	0.57	0.81	0.7	-0.8	-1.8	5.2	108	-104	156
CLIMBER-2	0.91	1.66	–	–	–	–	–	–	–
CLIMBER-3	0.91	1.55	–	–	–	–	–	–	–
DCESS	0.84	1.10	0.3	-0.9	-1.8	5.7	4	-102	258
GENIE	1.00	1.05	0.5	-1.4	-2.1	6.1	21	-114	251
IAPRASCM	0.80	–	–	–	–	–	–	–	–
IGSM	0.70	0.56	0.3	-0.7	-2.2	5.9	43	-122	237
LOVECLIM	0.38	0.67	–	–	–	–	–	–	–
MESMO	1.15	1.13	-0.6		-1.9	5.9	-28	-102	305
MIROC-lite-LCM	0.70	0.92	-0.1[a]		-1.6	5.4	108[b]	-86[b]	140[b]
UMD	0.79	1.56	-0.6		-2.4	6.2	-51	-136	347
UVic	0.75	1.43	1.3	-1.2	-2.0	5.2	24	-112	248
EMIC mean[c]	0.78[d]	1.13	0.6	-1.0	-1.9[d]	5.6	40	-111	230
EMIC range[c]	0.38 to 1.15	0.56 to 1.66	0.3 to 1.3	-1.4 to -0.7	-2.2 to -1.6	5.2 to 6.1	4 to 108	-122 to -102	156 to 258
Observed	0.73	0.8	1.6	-2.6	-2.2	6.4	39	-118	244
Uncertainty		0.5 to 1.1	0.5 to 2.7	-4.3 to -0.9	-2.6 to -1.8	6.0 to 6.8	11 to 67	-137 to -99	224 to 264

[a]Land-use change fluxes could not be diagnosed for this model because of the lack of a historical simulation with land-use change forcing only.

[b]Cumulative fluxes for this model are for 1851–1994.

[c]The MESMO and UMD models were excluded from the EMIC mean and range for the carbon cycle variables because they did not simulate land use change fluxes. Only the total land flux is reported for these models. The MIROC-lite-LCM model was excluded from the EMIC mean and range for the 1800–1994 cumulative fluxes because no carbon flux data was available prior to 1851.

[d]These values differ slightly from those reported in Eby et al. (2013) because of a different subset of EMICs included in the calculation.

TABLE 3. Global mean warming and thermal expansion relative to the 1986–2005 reference period for selected time periods and four RCPs. CMIP5 surface air temperature anomalies (Collins et al. 2013, Table 12.2) and thermal expansion (Church et al. 2013, Table 13.5) are shown for comparison. Listed are the model ensemble mean and the minimum and maximum values from the model distribution (in brackets). For CMIP5 thermal expansion the values in brackets span the likely range. EMIC year 2981–3000 values are from the constant-composition (CCO) simulations.

	2081–2100		2281–2300		2981–3000
Scenario	EMIC	CMIP5	EMIC	CMIP5	EMIC
			Warming (°C)		
RCP2.6	1.0 (0.6, 1.4)	1.0 (0.0, 2.0)	0.6 (0.3, 1.0)	0.7 (0.3, 1.4)	0.6 (0.3, 1.1)
RCP4.5	1.7 (0.9, 2.4)	1.8 (1.0, 2.8)	2.2 (1.3, 3.0)	2.6 (1.7, 3.9)	2.5 (1.7, 3.5)
RCP6.0	2.1 (1.1, 2.8)	2.3 (1.5, 3.2)	3.3 (1.9, 4.5)	4.2 (3.6, 4.9)	3.8 (2.6, 5.0)
RCP8.5	3.1 (1.6, 4.1)	3.7 (2.5, 5.0)	7.0 (3.8, 8.9)	8.6 (5.0, 14.1)	7.8 (4.7, 9.8)
			Thermal expansion (m)		
RCP2.6	0.14 (0.05, 0.20)	0.14 (0.10, 0.18)	0.22 (0.06, 0.37)	–	0.33 (0.09, 0.68)
RCP4.5	0.18 (0.09, 0.26)	0.19 (0.14, 0.23)	0.45 (0.17, 0.69)	–	0.82 (0.29, 1.64)
RCP6.0	0.20 (0.10, 0.29)	0.19 (0.15, 0.24)	0.62 (0.26, 0.95)	–	1.20 (0.47, 2.29)
RCP8.5	0.27 (0.13, 0.38)	0.27 (0.21, 0.33)	1.17 (0.64, 1.66)	–	2.48 (1.24, 4.31)

TABLE 4. Projected global mean warming and thermosteric sea level rise between 2300 and 3000 in constant-emissions (CEM), constant-composition (CCO), pre-industrial CO_2-emissions (PIEM-CO_2) and pre-industrial emission (PIEM) commitment simulations. Given are model ensemble means and model ranges (in brackets).

Scenario	CEM	CCO	PIEM-CO_2	PIEM
		Warming commitment (°C)		
RCP2.6	-0.8 (-1.0, -0.4)	0.0 (-0.1, 0.1)	-0.4 (-0.7, 0.4)	-0.8 (-1.2, 0.4)
RCP4.5	0.8 (0.5, 1.3)	0.3 (0.0, 0.6)	-0.5 (-1.0, 0.3)	-1.2 (-1.8, 0.3)
RCP6.0	1.1 (0.7, 1.4)	0.4 (0.0, 0.9)	-0.5 (-1.2, 0.4)	-1.2 (-2.0, 0.4)
RCP8.5	1.3 (0.7, 1.7)	0.7 (0.0,1.2)	-0.1 (-0.7, 0.6)	-1.3 (-2.3, 0.6)
		Thermal expansion commitment (m)		
RCP2.6	-0.04 (-0.10, 0.02)	0.11 (0.03, 0.32)	0.04 (-0.02, 0.15)	-0.03 (-0.09, 0.15)
RCP4.5	0.40 (0.16, 0.83)	0.38 (0.12, 0.95)	0.18 (0.02, 0.49)	0.08 (-0.08, 0.34)
RCP6.0	0.60 (0.24, 1.19)	0.57 (0.20, 1.34)	0.29 (0.04, 0.69)	0.16 (-0.07, 0.47)
RCP8.5	1.30 (0.41, 2.84)	1.31 (0.38, 2.64)	0.97 (0.22, 2.37)	0.66 (0.03, 1.69)

TABLE 5. Warming and thermosteric sea level in 3991–4000 relative to 1851–1860 for climate reversibility simulations with a 100-year ramp-down of atmospheric CO_2 after the year 3000 (REa), a 1000-year ramp-down of atmospheric CO_2 (REb) and freely evolving CO_2 (REc). Given are model ensemble means and model ranges (in brackets).

	Warming (°C)		
Scenario	REa	REb	REc
RCP2.6	0.4 (0.1,0.5)	0.5 (0.1,0.7)	1.3 (0.7,1.8)
RCP4.5	0.7 (0.5,0.9)	1.1 (0.6,1.4)	3.2 (2.2,4.0)
RCP6.0	0.9 (0.6,1.3)	1.4 (0.7,1.9)	4.5 (3.4,5.3)
RCP8.5	2.0 (1.1,4.3)	3.1 (1.5,4.6)	8.9 (6.7,10.2)
	Thermal expansion (m)		
RCP2.6	0.2 (0.05,0.4)	0.3 (0.1,0.7)	0.4 (0.1,0.8)
RCP4.5	0.3 (0.1,0.9)	0.5 (0.2,1.5)	0.8 (0.4,1.6)
RCP6.0	0.4 (0.1,1.1)	0.8 (0.3,2.0)	1.2 (0.6,2.4)
RCP8.5	0.8 (0.2,1.9)	1.9 (0.5,3.5)	2.9 (1.3,6.3)

List of Figures

5 Changes in carbon inventories by the year 3000 as a function of the change in atmospheric carbon between 1850 and 3000 for RCPs 2.6–8.5. (a) Cumulative carbon emissions since 1850, (b) airborne fraction of cumulative emissions, (c) land carbon uptake since 1850, (d) land uptake fraction, (e) ocean carbon uptake since 1850, (f) ocean uptake fraction. 54

6 Time evolution of climate variables under the pre-industrial CO_2-emission commitment simulations for four RCP scenarios: (a) Diagnosed cumulative CO_2 emissions since 1850, (b) atmospheric CO_2, (c) Surface air temperature change, (d) Ocean thermal expansion. Anomalies are relative to 1986–2005. Shown are the model ensemble averages (thick solid lines), the ranges spanned by all models (shaded domains, delimited by thin solid lines), and the range in the year 3000 (vertical bars on right hand side). Data were smoothed using a ten-year moving average. 55

7 RCP2.6 pre-industrial CO_2-emission commitment simulations. (a) Cumulative CO_2 emissions since 1850, (b) Atmospheric CO_2, (c) Surface air temperature change, (d) Ocean thermal expansion. Anomalies in panels (c) and (d) are relative to 1986–2005. Data in panel (c) were smoothed using a ten-year moving average. Note that the response of the UMD model differs from that of other models due to slightly positive CO_2 emissions after year 2300. 56

8 Pre-industrial CO_2-emission simulations for RCPs 2.6–8.5. (a) Atmospheric CO_2 in year 3000 as a fraction of atmospheric CO_2 in year 2300 (corresponding to peak atmospheric CO_2 in RCPs 4.5–8.5), (b) Warming in year 3000 as a fraction of warming in year 2300 (corresponding approximately to peak warming in RCPs 4.5–8.5). Results are shown as a function of the peak atmospheric CO_2 concentration in each RCP, which is the same for all models. 57

9 Time evolution of climate variables under the pre-industrial emission commitment simulations for four RCP scenarios: (a) atmospheric CO_2, (b) Surface air temperature change, (c) Ocean thermal expansion. Anomalies are relative to 1986–2005. Shown are the model ensemble averages (thick solid lines), the ranges spanned by all models (shaded domains, delimited by thin solid lines), and the range in the year 3000 (vertical bars on right hand side). Data were smoothed using a ten-year moving average. 58

10 Time evolution of climate variables for constant-CO_2-emission commitment simulations under four RCP scenarios: (a) Diagnosed CO_2 emissions, (b) atmospheric CO_2, (c) Surface air temperature change, (d) Ocean thermal expansion. Anomalies in panels (c) and (d) are relative to 1986–2005. Shown are the model ensemble averages (thick solid lines), the ranges spanned by all models (shaded domains, delimited by thin solid lines), and the range in the year 3000 (vertical bars on right hand side). Data were smoothed using a ten-year moving average. 59

11 Time evolution of climate variables for reversibility simulations with atmospheric CO_2 after year 3000 decreasing to pre-industrial levels over 100 years: (a) Atmospheric CO_2, (b) Surface air temperature change, (c) Ocean thermal expansion, (d) Atlantic overturning index (maximum of the overturning streamfunction in the North Atlantic). Anomalies in panels (b) and (c) are relative to pre-industrial (1851–1860). Shown are the model ensemble averages (thick solid lines), the ranges spanned by all models (shaded domains, delimited by thin solid lines), and the range in the year 3000 (vertical bars on right hand side). Data were smoothed using a ten-year moving average. 60

12 Time evolution of climate variables for reversibility simulations with atmospheric CO_2 after year 3000 decreasing to pre-industrial levels over 1000 years: (a) Atmospheric CO_2, (b) Surface air temperature change, (c) Ocean thermal expansion, (d) Atlantic meridional overturning index Atlantic overturning index (maximum of the overturning streamfunction in the North Atlantic). Anomalies in panels (b) and (c) are relative to pre-industrial (1851–1860). Shown are the model ensemble averages (thick solid lines), the ranges spanned by all models (shaded domains, delimited by thin solid lines), and the range in the year 3000 (vertical bars on right hand side). Data were smoothed using a ten-year moving average. 61

13 Time evolution of climate variables for reversibility simulations with atmospheric CO_2 after year 3000 evolving freely (zero emissions). These experiments were performed by EMICs with an interactive carbon cycle only: (a) Atmospheric CO_2, (b) Surface air temperature change, (c) Ocean thermal expansion, (d) Atlantic overturning index (maximum of the overturning streamfunction in the North Atlantic). Anomalies in panels (b) and (c) are relative to pre-industrial (1851–1860). Shown are the model ensemble averages (thick solid lines), the ranges spanned by all models (shaded domains, delimited by thin solid lines), and the range in the year 3000 (vertical bars on right hand side). Data were smoothed using a ten-year moving average. 62

14 Diagnosed CO_2 emissions for reversibility simulations with atmospheric CO_2 after year 3000 decreasing to pre-industrial levels over 100 years (a), and 1000 years (b). Results are shown for seven EMICs with an interactive carbon cycle. Shown are the model ensemble averages (thick solid lines), the ranges spanned by all models (shaded domains, delimited by thin solid lines), and the range in the year 3000 (vertical bars on right hand side). Note the different vertical scales in panels (a) and (b). 63

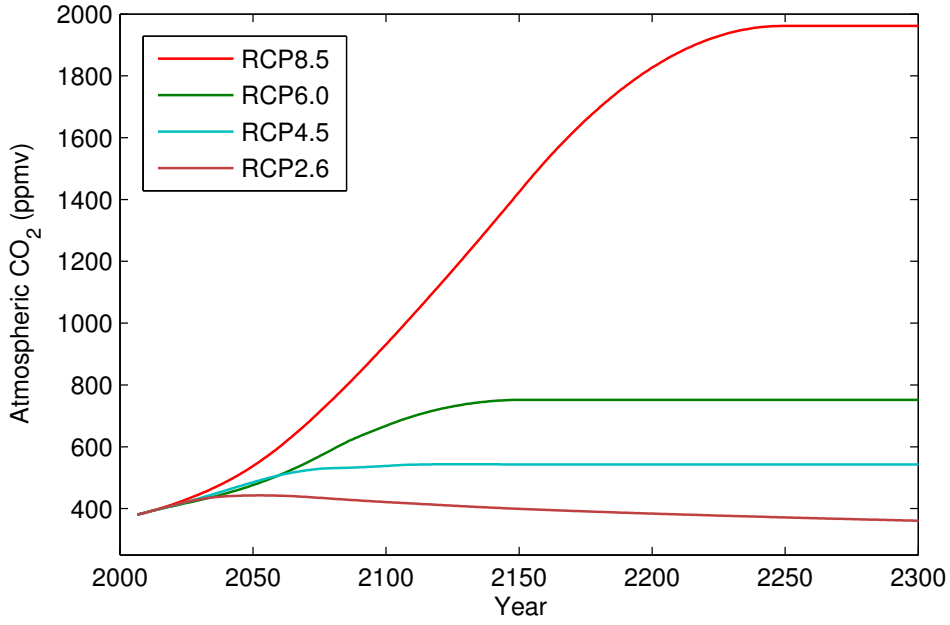

FIG. 1. Time evolution of atmospheric CO_2 between 2006 and 2300 for the four RCP scenarios and their extensions (RCP database version 2.0, https://www.iiasa.ac.at/web-apps/tnt/RcpDb/).

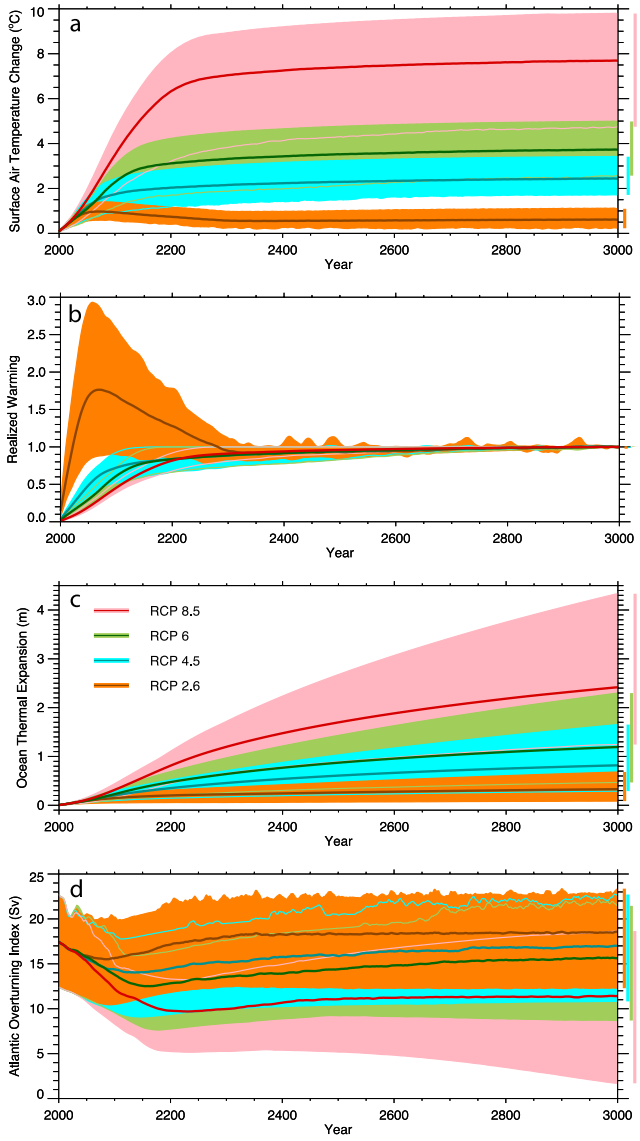

FIG. 2. Constant composition commitment. Time evolution of physical climate variables for four RCP scenarios: (a) Surface air temperature change, (b) Fraction of realized warming (calculated as the ratio of warming at any time to the warming averaged over 2981–3000), (c) Ocean thermal expansion, (d) Atlantic overturning index, defined as the maximum value of the overturning streamfunction in the North Atlantic. Anomalies are relative to 1986–2005. Shown are the model ensemble averages (thick solid lines), the ranges spanned by all models (shaded domains, delimited by thin solid lines), and the range in the year 3000 (vertical bars on right hand side). Data were smoothed using a ten-year moving average.

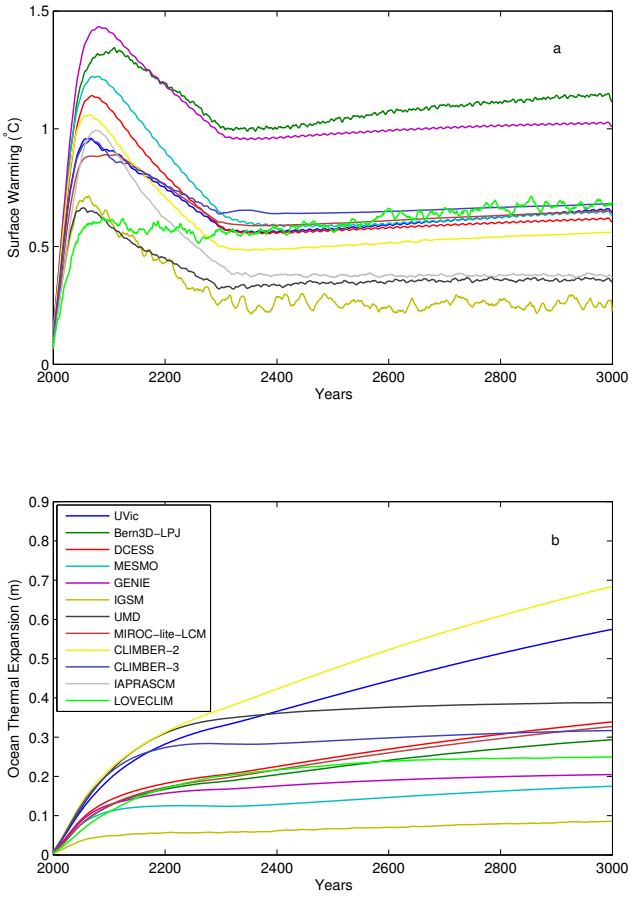

FIG. 3. RCP2.6 constant composition commitment simulations. (a) Surface air temperature change, (b) Ocean thermal expansion. Anomalies are relative to 1986–2005. Data in panel (a) were smoothed using a ten-year moving average.

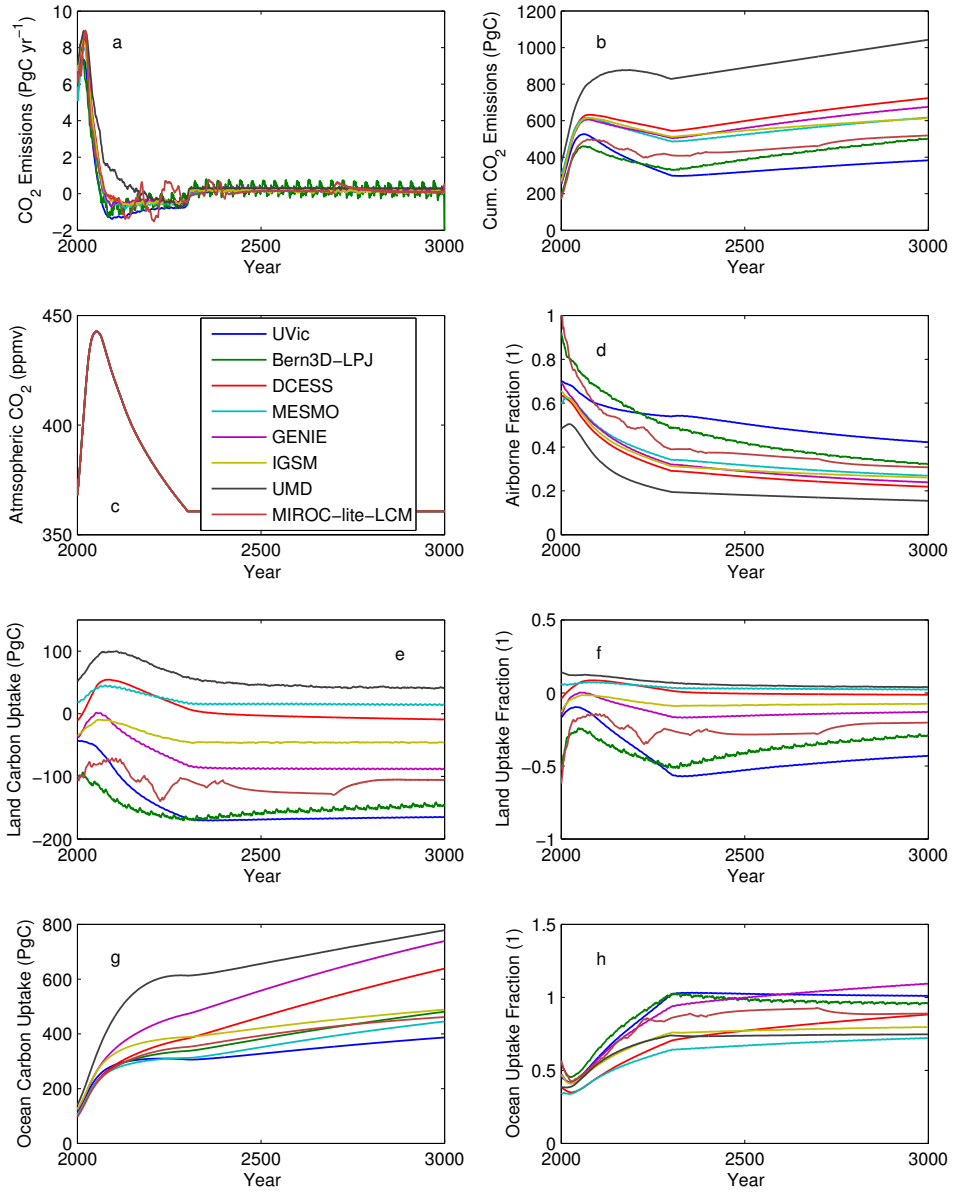

FIG. 4. Changes in carbon inventories in RCP2.6 constant composition commitment simulations for eight EMICs with an interactive carbon cycle. (a) CO_2 emissions, (b) Cumulative CO_2 emissions since 1850, (c) Atmospheric CO_2 concentration, (d) Airborne fraction of cumulative emissions, (e) Land uptake since 1850, (f) Fraction of cumulative emissions taken up by land, (g) Ocean uptake since 1850, (h) Fraction of cumulative emissions taken up by ocean. Note that for individual models the ocean uptake fraction can be > 1 if the land uptake fraction is < 0. Data in panel (a) were smoothed using a ten-year moving average.

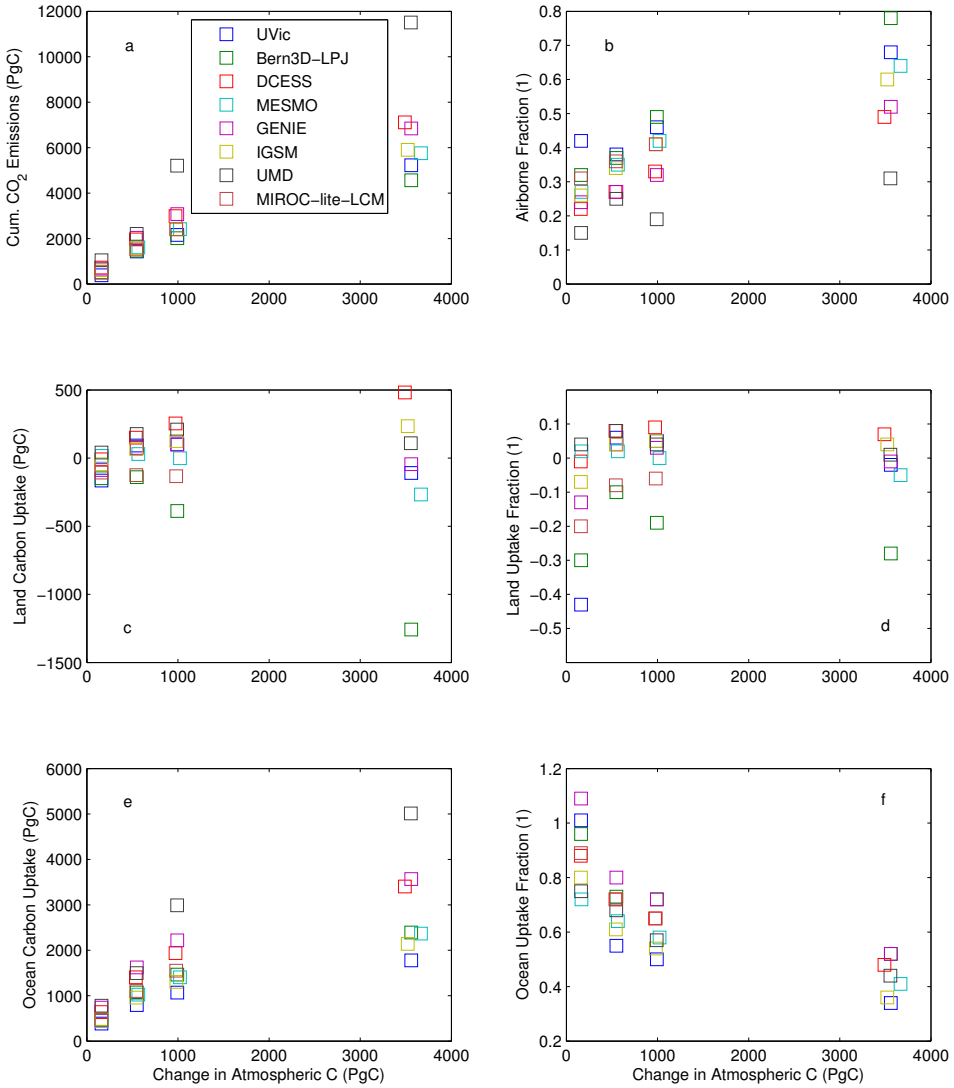

FIG. 5. Changes in carbon inventories by the year 3000 as a function of the change in atmospheric carbon between 1850 and 3000 for RCPs 2.6–8.5. (a) Cumulative carbon emissions since 1850, (b) airborne fraction of cumulative emissions, (c) land carbon uptake since 1850, (d) land uptake fraction, (e) ocean carbon uptake since 1850, (f) ocean uptake fraction.

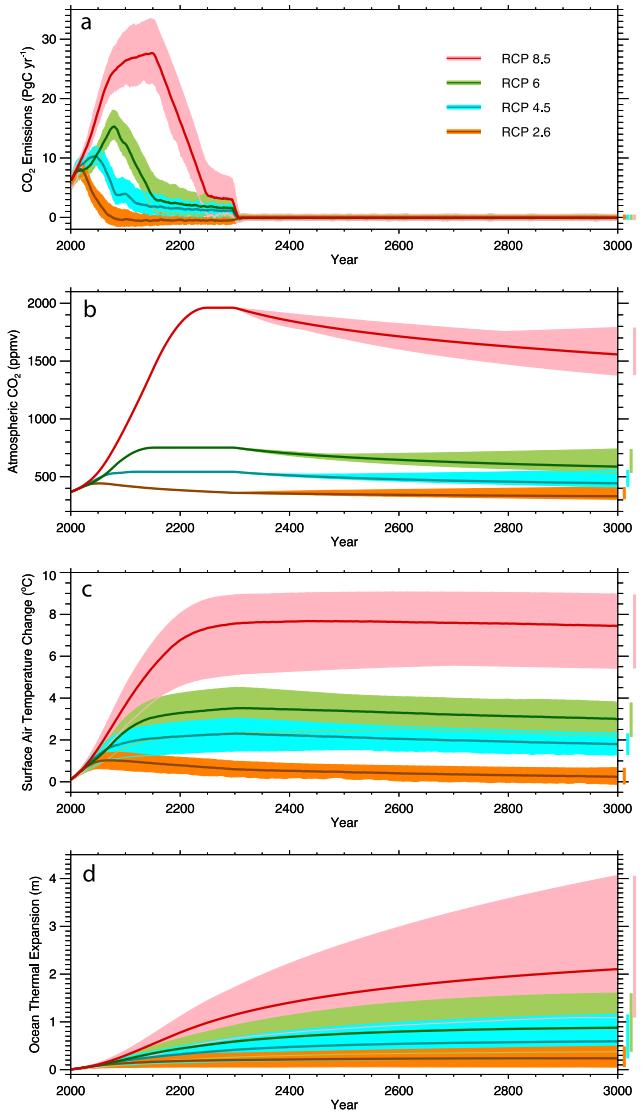

FIG. 6. Time evolution of climate variables under the pre-industrial CO_2-emission commitment simulations for four RCP scenarios: (a) Diagnosed cumulative CO_2 emissions since 1850, (b) atmospheric CO_2, (c) Surface air temperature change, (d) Ocean thermal expansion. Anomalies are relative to 1986–2005. Shown are the model ensemble averages (thick solid lines), the ranges spanned by all models (shaded domains, delimited by thin solid lines), and the range in the year 3000 (vertical bars on right hand side). Data were smoothed using a ten-year moving average.

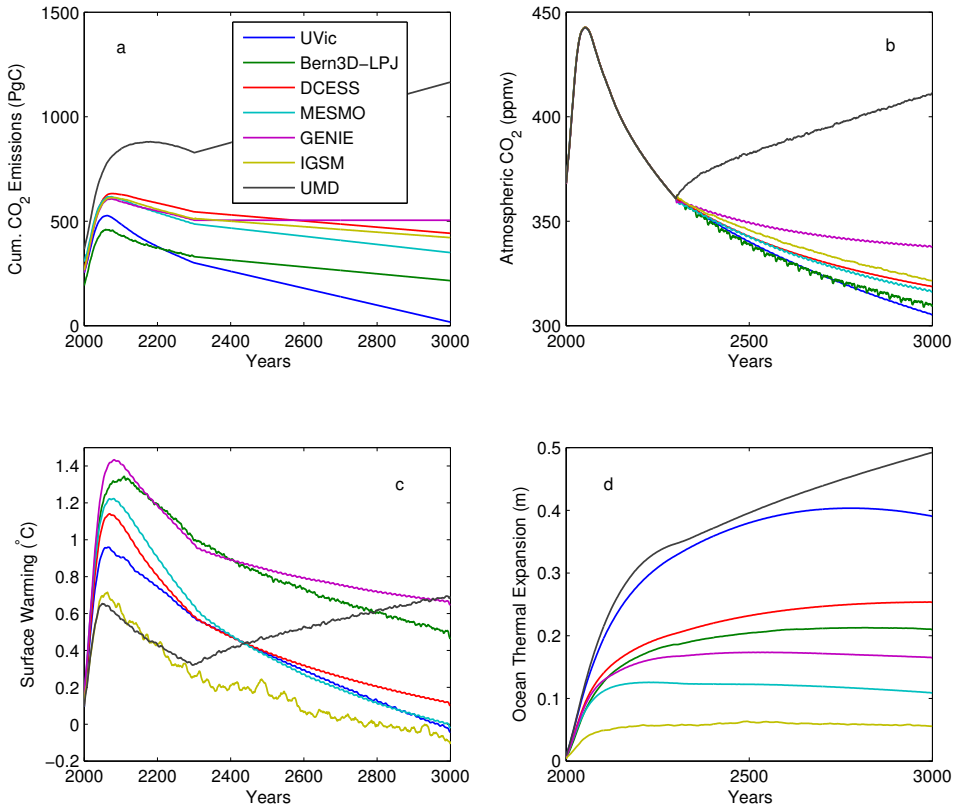

FIG. 7. RCP2.6 pre-industrial CO_2-emission commitment simulations. (a) Cumulative CO_2 emissions since 1850, (b) Atmospheric CO_2, (c) Surface air temperature change, (d) Ocean thermal expansion. Anomalies in panels (c) and (d) are relative to 1986–2005. Data in panel (c) were smoothed using a ten-year moving average. Note that the response of the UMD model differs from that of other models due to slightly positive CO_2 emissions after year 2300.

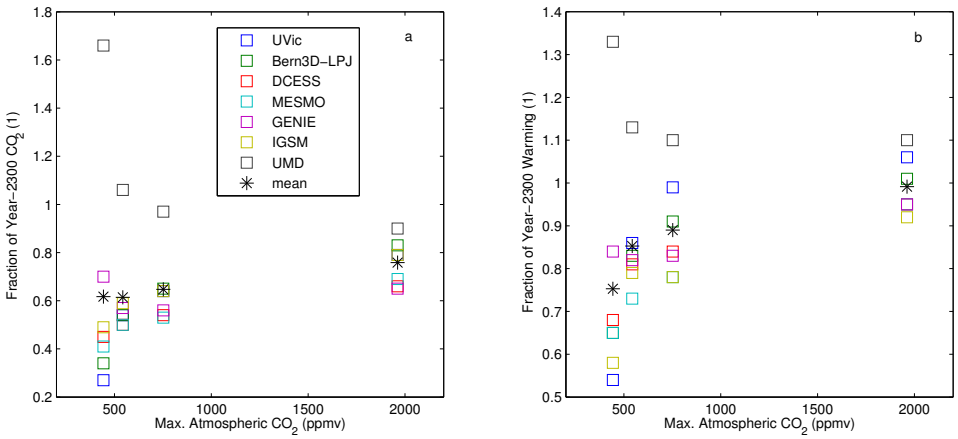

FIG. 8. Pre-industrial CO_2-emission simulations for RCPs 2.6–8.5. (a) Atmospheric CO_2 in year 3000 as a fraction of atmospheric CO_2 in year 2300 (corresponding to peak atmospheric CO_2 in RCPs 4.5–8.5), (b) Warming in year 3000 as a fraction of warming in year 2300 (corresponding approximately to peak warming in RCPs 4.5–8.5). Results are shown as a function of the peak atmospheric CO_2 concentration in each RCP, which is the same for all models.

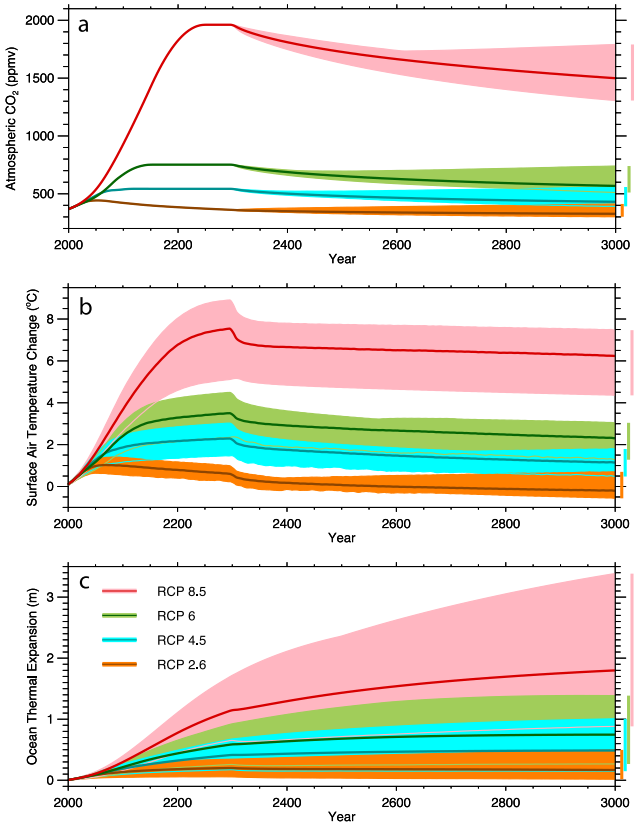

FIG. 9. Time evolution of climate variables under the pre-industrial emission commitment simulations for four RCP scenarios: (a) atmospheric CO_2, (b) Surface air temperature change, (c) Ocean thermal expansion. Anomalies are relative to 1986–2005. Shown are the model ensemble averages (thick solid lines), the ranges spanned by all models (shaded domains, delimited by thin solid lines), and the range in the year 3000 (vertical bars on right hand side). Data were smoothed using a ten-year moving average.

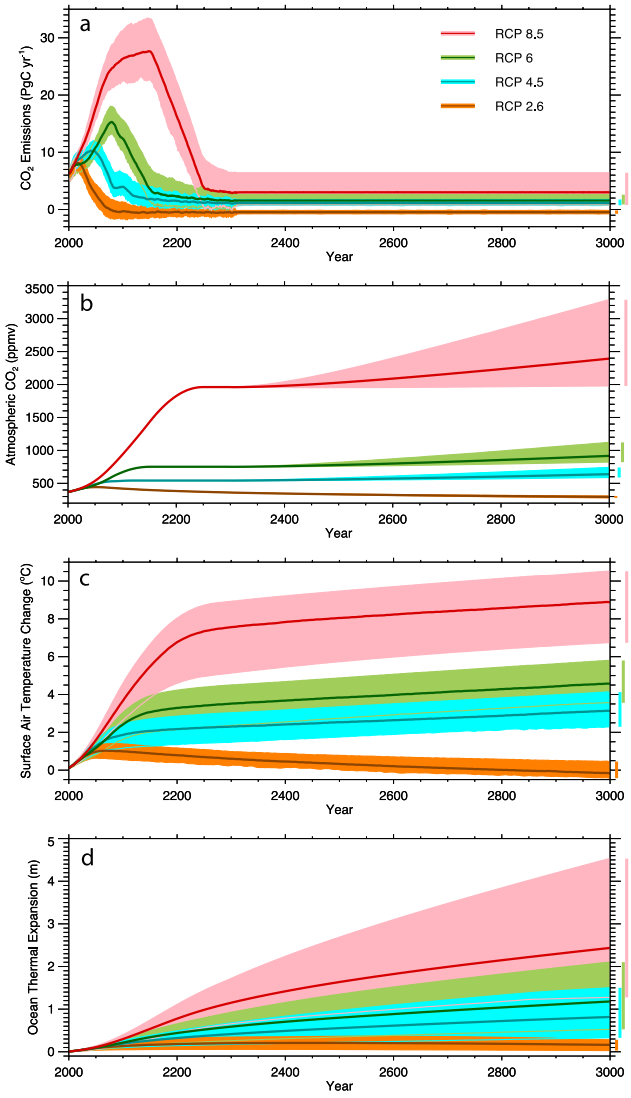

FIG. 10. Time evolution of climate variables for constant-CO_2-emission commitment simulations under four RCP scenarios: (a) Diagnosed CO_2 emissions, (b) atmospheric CO_2, (c) Surface air temperature change, (d) Ocean thermal expansion. Anomalies in panels (c) and (d) are relative to 1986–2005. Shown are the model ensemble averages (thick solid lines), the ranges spanned by all models (shaded domains, delimited by thin solid lines), and the range in the year 3000 (vertical bars on right hand side). Data were smoothed using a ten-year moving average.

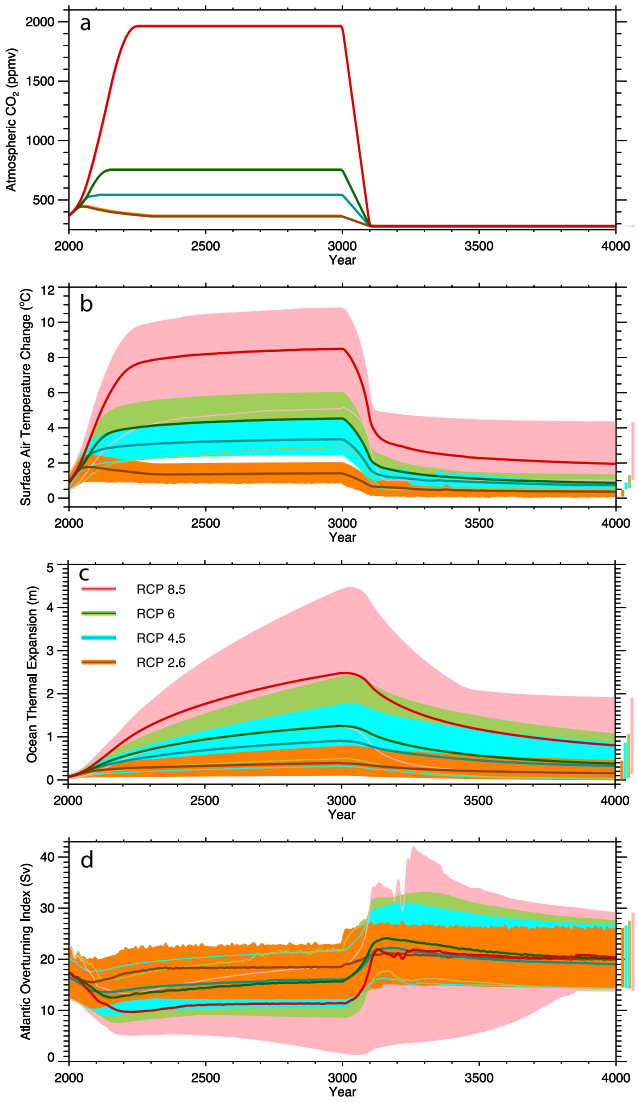

FIG. 11. Time evolution of climate variables for reversibility simulations with atmospheric CO_2 after year 3000 decreasing to pre-industrial levels over 100 years: (a) Atmospheric CO_2, (b) Surface air temperature change, (c) Ocean thermal expansion, (d) Atlantic overturning index (maximum of the overturning streamfunction in the North Atlantic). Anomalies in panels (b) and (c) are relative to pre-industrial (1851–1860). Shown are the model ensemble averages (thick solid lines), the ranges spanned by all models (shaded domains, delimited by thin solid lines), and the range in the year 3000 (vertical bars on right hand side). Data were smoothed using a ten-year moving average.

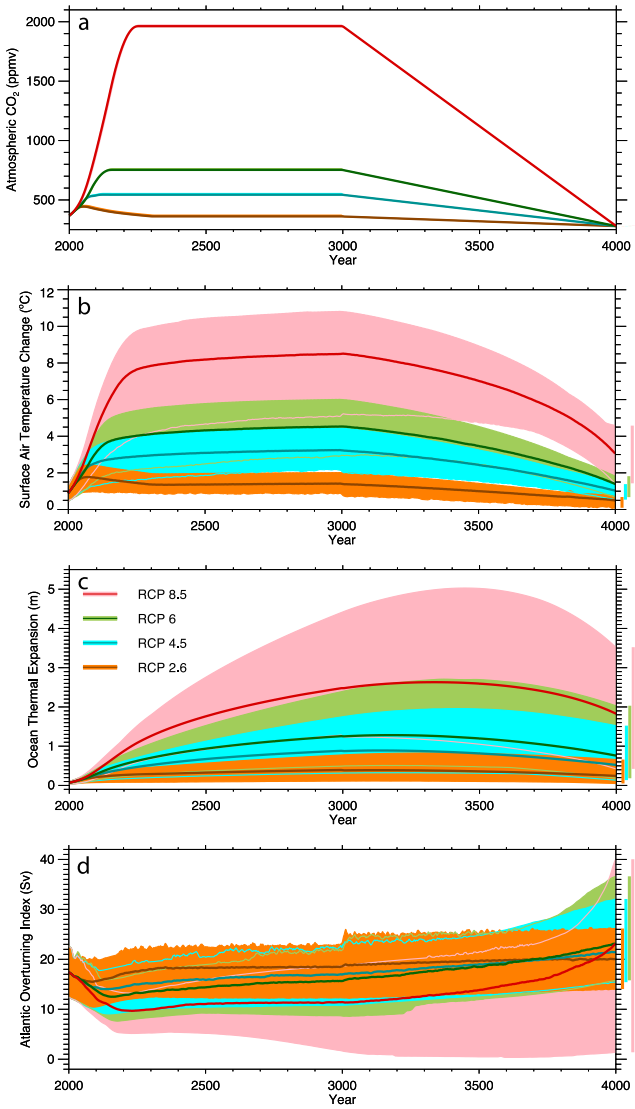

FIG. 12. Time evolution of climate variables for reversibility simulations with atmospheric CO_2 after year 3000 decreasing to pre-industrial levels over 1000 years: (a) Atmospheric CO_2, (b) Surface air temperature change, (c) Ocean thermal expansion, (d) Atlantic meridional overturning index Atlantic overturning index (maximum of the overturning streamfunction in the North Atlantic). Anomalies in panels (b) and (c) are relative to pre-industrial (1851–1860). Shown are the model ensemble averages (thick solid lines), the ranges spanned by all models (shaded domains, delimited by thin solid lines), and the range in the year 3000 (vertical bars on right hand side). Data were smoothed using a ten-year moving average.

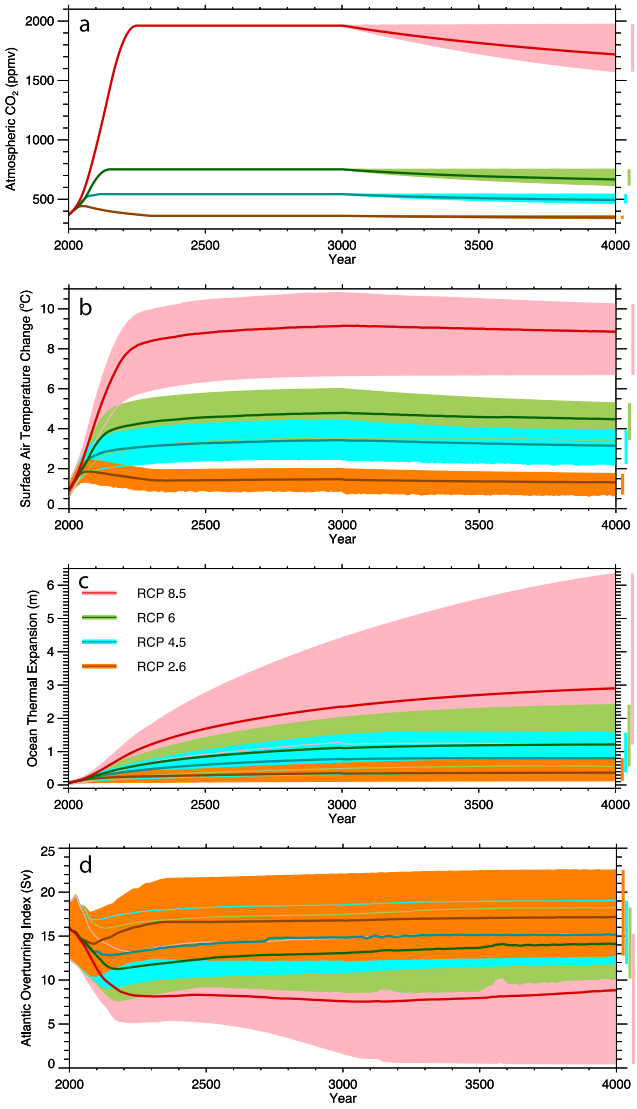

FIG. 13. Time evolution of climate variables for reversibility simulations with atmospheric CO_2 after year 3000 evolving freely (zero emissions). These experiments were performed by EMICs with an interactive carbon cycle only: (a) Atmospheric CO_2, (b) Surface air temperature change, (c) Ocean thermal expansion, (d) Atlantic overturning index (maximum of the overturning streamfunction in the North Atlantic). Anomalies in panels (b) and (c) are relative to pre-industrial (1851–1860). Shown are the model ensemble averages (thick solid lines), the ranges spanned by all models (shaded domains, delimited by thin solid lines), and the range in the year 3000 (vertical bars on right hand side). Data were smoothed using a ten-year moving average.

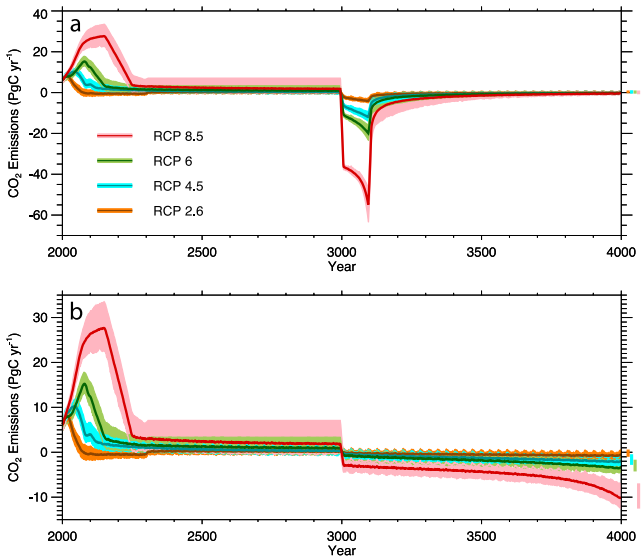

FIG. 14. Diagnosed CO_2 emissions for reversibility simulations with atmospheric CO_2 after year 3000 decreasing to pre-industrial levels over 100 years (a), and 1000 years (b). Results are shown for seven EMICs with an interactive carbon cycle. Shown are the model ensemble averages (thick solid lines), the ranges spanned by all models (shaded domains, delimited by thin solid lines), and the range in the year 3000 (vertical bars on right hand side). Note the different vertical scales in panels (a) and (b).

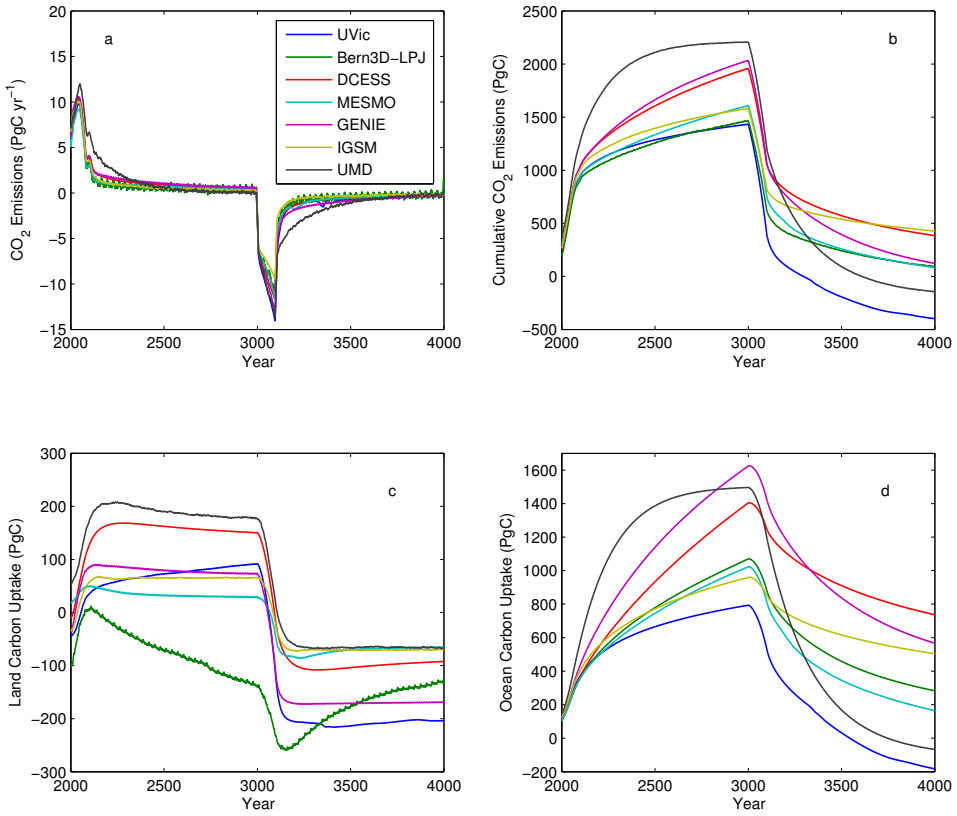

FIG. 15. Changes in carbon inventories for the RCP4.5 reversibility simulation with atmospheric CO_2 after year 3000 decreasing to pre-industrial levels over 100 years. (a) CO_2 emissions, (b) Cumulative CO_2 emissions since 1850, (c) Land uptake since 1850, (d) Ocean uptake since 1850. Data in panel (a) were smoothed using a ten-year moving average.

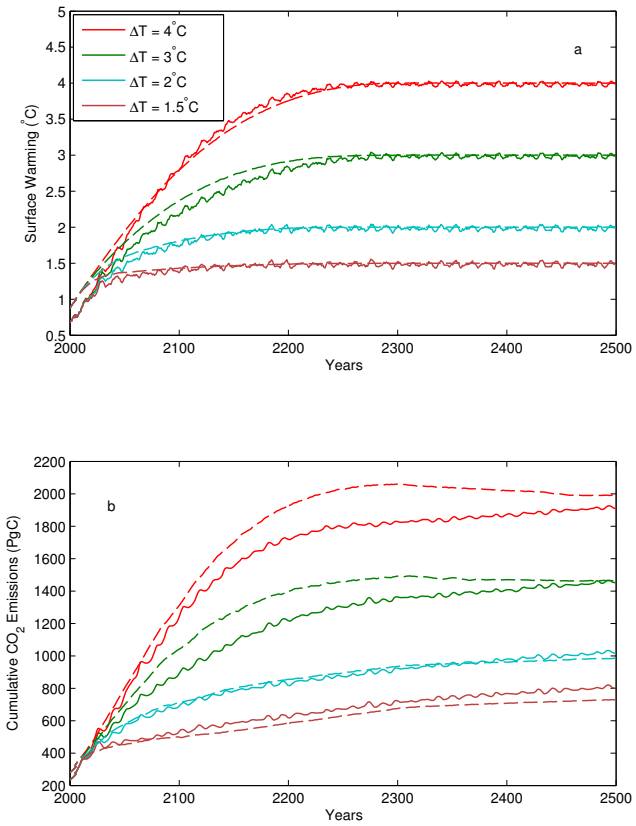

FIG. 16. Cumulative CO_2 emissions compatible with a set of long-term temperature targets (1.5–4°C) for temperature tracking experiments with two EMICs: UVic (dashed) and Bern3D-LPJ (solid). (a) Surface air temperature change relative to pre-industrial (1800 for UVic, 850 for Bern3D-LPJ), (b) Cumulative CO_2 emissions since pre-industrial.

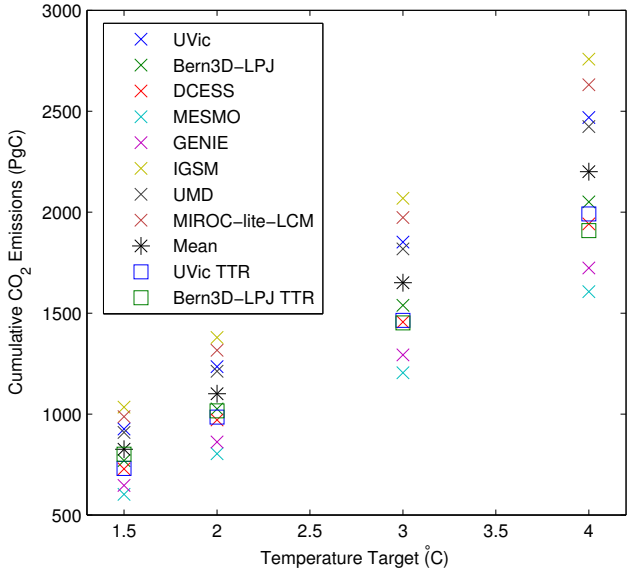

FIG. 17. Cumulative CO_2 emissions compatible with a set of long-term temperature targets (1.5–4°C) for EMICs with an interactive carbon cycle. Allowable cumulative emissions are derived from the models' Climate Carbon Response (CCR) given in Table 4 of Eby et al. (2013). Also shown are the year-2500 cumulative emissions derived from temperature tracking experiments (TTR) with the UVic and Bern3D-LPJ EMICs (square symbols).